Chapter 2
Size and Shape Control Synthesis of Iron Oxide–Based Nanoparticles: Current Status and Future Possibility

Khuram Ali, Yasir Javed, and Yasir Jamil

2.1 Introduction

Magnetic phenomena at the atomic scale were discovered in the early twentieth century, whereas the discovery of the first known magnetic material (Fe_3O_4) revolutionized the field of magnetism. The magnetic properties of a material depend on temperature, the applied magnetic field, and pressure. A change in these variables will result in the existence of two or more forms of magnetism. Ferro- and ferrimagnetic materials like Fe_3O_4 and some of their alloys have particles whose shape is asymmetrical when they are obtained by the grinding of bulk materials, whereas they can possess a spherical shape only when manufactured through plasma atomization or wet chemistry or when in aerosol and gas phases. Depending on the procedure used to form particles, they can be crystalline or amorphous spherical in shape. To a large extent, the synthesis process determines the degree of impurities in a particle, as well as the presence of structural defects, and, hence, the division of these defects inside the particle structure can be used to discover its magnetic properties [1, 2].

Magnetization depends on the number of unpaired valence electrons present in the atoms of solids and on the relative orientations of the neighboring magnetic moments [3]. Two types of motion of electrons in atoms are responsible for magnetism. One is the spin of electrons around the atom's axis, and the other is the motion of electrons in an orbit around the nucleus. Iron (Fe), nickel (Ni), manganese (Mn), and cobalt (Co) are magnetic materials that have a net magnetic moment. In transition metal atoms, the magnetic moment is due to electron spin [4].

K. Ali (✉) • Y. Javed • Y. Jamil
Nano-Optoelectronics Research Laboratory, Department of Physics, University of Agriculture Faisalabad, Faisalabad 38040, Pakistan
e-mail: khuram_uaf@yahoo.com; myasi60@gmail.com; yasirjamil@yahoo.com

S.K. Sharma (ed.), *Complex Magnetic Nanostructures*,
DOI 10.1007/978-3-319-52087-2_2

2.1.1 Classification of Magnetic Materials

In solids, materials may be categorized by their response to an externally applied magnetic field. There are five basic types of magnetism, paramagnetism, diamagnetism, ferromagnetism, ferrimagnetism, and antiferromagnetism. The magnetic properties of a material are governed by the electronic structure of the atoms within the material. They vary from weakly magnetic (diamagnetic) to permanently magnetic (ferromagnetic).

The most important property of a magnetic material is the magnetic susceptibility (χ), defined by

$$\chi = \frac{M}{H}, \tag{2.1}$$

where M is the magnetization and H the magnetic field, both of which are measured in units of A/m. In general, the magnetic susceptibility is different for each material, temperature dependent (except in diamagnetic materials), and of the form

$$\chi = \frac{C}{T \pm \theta}. \tag{2.2}$$

2.1.1.1 Diamagnetism

Diamagnetism is a basic property of all matter, but it is an extremely weak property. The susceptibility (χ) is negative and on the order of approximately 10^{-5}. The other characteristic behavior of diamagnetic materials is that their susceptibility is independent of temperature. The origin of diamagnetism is due to the noncooperative behavior of orbiting electrons when exposed to an applied external magnetic field. Diamagnetic materials are composed of atoms having no net magnetic moments (i.e., all the orbital shells are filled and there are no unpaired electrons). When a small field is applied, a small negative magnetization is generated that is proportional to the applied field strength (Fig. 2.1a).

2.1.1.2 Paramagnetism

Because of the magnetic field generated by unpaired electrons, atoms may behave like magnets under the influence of an external magnetic field. However, when the applied magnetic field is removed, the thermal fluctuations would cause the magnetic moment of paramagnetic atoms to move randomly. In the presence of a relatively low magnetic field, this effect can be described by Curie's law,

$$\chi_{\text{para}} = \frac{M}{H} = \frac{C}{T}, \tag{2.3}$$

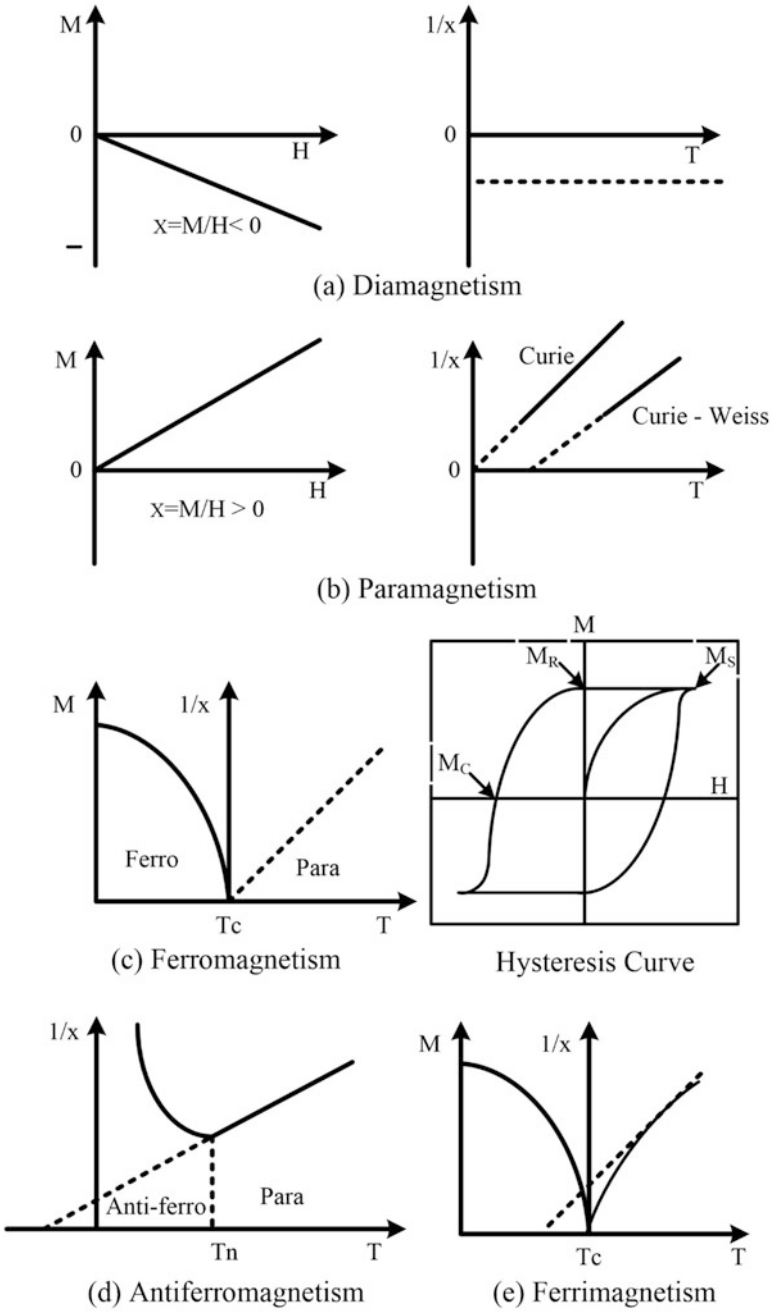

Fig. 2.1 (**a**–**e**) Different kinds of magnetism and their main behavior

where C is the Curie constant. The expected behaviors of paramagnetic materials with an applied external magnetic field and with temperature are shown in Fig. 2.1b. In general, the response of a material to a magnetic field, that is, the magnetic susceptibility (χ), is on the order of 10^{-3}–10^{-5}.

2.1.1.3 Ferromagnetism

Ferromagnetic materials exhibit parallel alignment of magnetic moments to one another, resulting in a large net magnetization, even in zero magnetic fields, known as spontaneous magnetization. The atomic dipole moments in these materials are characterized by very strong positive interactions produced by electronic exchange forces, which results in a parallel alignment of atomic moments. The two distinct features of ferromagnetic materials are a magnetic ordering temperature and spontaneous magnetization.

Ferromagnetism is strongly temperature dependent, and the magnetization of a ferromagnetic material is inversely proportional to temperature by the Curie–Weiss law:

$$\chi = \frac{C}{T - \theta}. \tag{2.4}$$

The Curie temperature is the temperature above which exchange forces cease to be present, that is, above that temperature a ferromagnetic material randomizes owing to the thermal energy, as in paramagnetic systems (Fig. 2.1c). They have relatively large susceptibilities, and in general, magnetic saturation is achieved through fields lower than for paramagnetic systems by a factor of 10^4.

2.1.1.4 Antiferromagnetism

Antiferromagnetic materials are characterized by a weak magnetic susceptibility of the order of paramagnetic materials. In a simple antiferromagnetic material, the atoms can be divided into two sublattices, where magnetic dipole moments are aligned antiparallel, which causes a small magnetic susceptibility in these materials. The temperature above which antiferromagnetic order ceases to exist is called the Neel (T_N) temperature (Fig. 2.1d). Above T_N, antiferromagnetic materials have a slight positive susceptibility comparable to that of paramagnetic materials. Below T_N, however, antiferromagnetic materials have a spontaneous magnetization in the absence of an external field that causes the magnetic dipole moments of sublattices to align antiparallel to each other.

2.1.1.5 Ferrimagnetism

Ferrimagnetic materials, like ferromagnetic materials, have a spontaneous magnetization below a critical temperature called the Curie temperature (T_C). The magnitude of the magnetic susceptibility (χ) of ferro-/ferrimagnetic materials is identical, while the alignment of magnetic dipole moments is drastically different (Fig. 2.1e). The magnetic dipole moments in a ferrimagnetic material are divided into two sublattices and classified as a subset of antiferromagnetic materials. Each sublattice can be treated as a ferromagnetic material, and the difference between the magnetic dipole moments for the sublattices results in a net magnetization for ferrimagnetic materials. The major difference between ferrimagnetic and antiferromagnetic materials is that either the magnitude or the number of moments of sublattices is different.

The most important crystalline ferrimagnetic substances are double oxides of iron, as in $MO.Fe_2O_3$, where M is a divalent metal. These are based on the spinel structure; the protypical example is magnetite, Fe_3O_4. As the temperature rises, the alignment of the spins is disturbed by thermal energy and the magnetization decreases. At a certain temperature, called the Curie temperature T_C, this alignment becomes completely disordered and the magnetization vanishes.

2.1.1.6 Superparamagnetism

Superparamagnetic materials are a special class of magnetic materials. They are single-domain particles that behave like ordinary ferromagnetic materials below T_C because they have rather large magnetic susceptibilities, are saturated in moderate magnetic fields, and display coercivity and remanence. Above T_C, however, superparamagnetic materials behave like ordinary paramagnetic materials in that they display no hysteresis (i.e., no coercivity or remanence).

The idea of superparamagnetism was first developed and proposed by Neel [5, 6] to describe the possibility of thermal fluctuations in single-domain ferromagnetic clusters. In general, the magnetic anisotropy energy of a particle is proportional to its volume. In a given crystal of volume V, the magnetic anisotropy energy is given by

$$E_A = KV\sin^2\theta, \tag{2.5}$$

where K is the anisotropy energy constant and θ the angle between the magnetization vector and easy axis of nanoparticles [7]. When the volume of a single-domain cluster is small enough, the magnetic anisotropy energy of the cluster approaches its thermal energy, causing the magnetization to flip between easy axes through an anisotropy barrier in the same way as in a classical paramagnetic system [8] but, with a giant magnetic moment, that of a single atom, hence the term *superparamagnetism*.

2.1.2 Ferrites

Ferrites are considered a very important class of oxides with significant magnetic properties. Ferrites have been widely studied and applied over the past several decades. To say that ferrites have magnetic properties means they will attract magnets of opposite polarity and iron-based alloys and repel magnets of similar polarity. Ferrites also possess dielectric properties, which mean that they do not conduct electricity when electromagnetic waves pass through them. In various applications, this gives them an advantage over Ni, Fe, and transition metals that possess magnetic properties ("ferromagnetic") because these metals conduct electricity when electromagnetic waves pass through them [9]. The phenomenon of *ferromagnetic* ferrites is the converse of *ferromagnetic* metals. In ferrimagnetism, there is not just one arrangement but distinct alignments of perpendicular and parallel magnetic moments. It is these alignments that give them their remarkable properties. This property can be attained through various crystal structures [10].

2.1.2.1 Applications of Ferrites

Ferrites have applications in such devices as antenna cores, transformers and tuned inductors, compasses, injection pumps, starter motors, loudspeakers, antilock braking systems, microphones, eddy current brakes, telephone rings, switches, alternators, stepping motors, drills, clocks, printers, washing machines, computers, sensors, dampers, energy meter discs, electrochemical transducers, nuclear magnetic resonance spectrometers, DC motors for magnetic devices, magnetic bearings, robotics, clutches and brakes, coupling, orthodontics, instrumentation, lifting apparatus, cancer cell separators, wound closures, magnetic resonance imaging (MRI) body scanners, and ferromagnetic probes. Ferrites are mainly used as inductive components in electronic circuits like impedance matching networks, filters, and low-noise amplifiers. Ferrites have various power applications, such as video and TV systems, computers, and both medium-sized and small gadgets [11, 12].

2.1.2.2 Types of Ferrites

Ferrites are mainly categorized into two major groups, hard ferrites and soft ferrites. In 1945, the first so-called soft ferrite was produced by J. L. Snoek in the Netherlands for commercial purposes [13]. Ferrites are produced in specific sizes and shapes and used for antenna applications, and soft ferrites have multiplied in number and in terms of shapes and sizes. Ferrites have wide applications in electronics, and ferrite devices are the best choice for both modern and conventional applications because of their low cost and because of the continuous improvements being made in their material properties [14].

The magnetic field strength of soft ferrites decreases with time, so their magnetization is temporary. Soft ferrites have numerous applications, such as in inductors, radio frequency interference filters, and transformers [15]. Soft ferrites are a type of black and gray ceramic material and are brittle, inert, and hard. Soft ferrites possess a spinel structure. The usual composition of ferrites is $MeFe_2O_4$, where Me denotes one or more divalent metals like Mg, Mn, Cu, Ni, Fe, and Zn. Soft magnets can become magnetized when drawn toward another magnet, that is, they possess an obvious magnetism only when they are in a magnetic field. They are not permanently magnetized and are used in applications such as cores of distribution power transformers, rotor and stator materials for generators, and motors and electronic transformers [16].

Magnetite (Fe_2O_3) is a weak hard ferrite. Hard ferrites have a basically permanent magnetism. Over time, artificial hard ferrites with fine characteristics were acquired but in the laboratory, with an analogous soft magnetic material being fabricated. A hard magnet attracts other magnetized materials to itself. It retains this obvious magnetism, more or less permanently.

Hard ferrites are mostly used as permanent magnets in brushless and synchronous motors, loudspeakers, and telephone receivers. Hard magnets or hard ferrites also behave as permanent magnets. Hard ferrites are magnetic materials that retain their magnetism after being magnetized. Generally such materials have a very high coercivity (>10 kA/m) [17].

Currently, the most significant use of ferrites is as a medium for the transmission of microwaves. At very high frequencies (above approximately 500 MHz, and in the range of 1–30 GHz), some ferrites show a nonreciprocal effect. This means that electromagnetic waves passing through ferrites behave differently and travel in different directions. This phenomenon is used to construct one-way transmission lines, junctions to control microwave "traffic," and other microwave-controlled appliances. Today, the latest telecommunications systems would not be possible without ferrites. Ferrites are studied extensively, for example, because of their applications at high frequencies and in low eddy current losses, their usefulness at microwave frequencies and mechanical stiffness, and the high coercivity of selected ferrites; in addition, ferrites are used as insulators with magnetic properties, and some ferrites have square hysteresis loops. On the basis of their crystalline structure, ferrites are categorized into four main classes: cubic or spinel ferrites, hexaferrites, orthoferrites, and garnets [18].

2.2 Structural and Magnetic Properties of Nanomaterials

This section aims to provide an understanding of the structural properties of nanomaterials since their technologically relevant properties depend on their structure at the nanoscale.

2.2.1 Crystal Structures

For iron, there are 16 different forms of oxide. In 13 compounds, iron is in its trivalent form, while in the three remaining compounds, −FeO, $-Fe(OH)_2$, and Fe_3O_4, it is in divalent form. All oxides, hydroxides, and oxide hydroxides (or oxyhydroxides) of iron have a crystalline structure. Iron oxides are usually arranged in close packed lattices in hexagonal (hcp) or cubic (ccp) arrangements, where interstitial sites are partially filled by Fe^{2+} or Fe^{3+}, mostly in octahedral sites, and in a few cases in a tetrahedral geometry. The iron oxide structures are described here.

2.2.1.1 Magnetite (Fe_3O_4)

Magnetite occurs in nature as magnetic ore, known as lodestone. Magnetite differs from the majority of other iron oxides in that it contains both trivalent and divalent iron ions. Both magnetite and maghemite have an inverse spinel structure, and differentiating between the two structures in diffraction patterns remains a challenge [19]. Magnetite has a face-centered cubic (fcc) structure on 30 O^{2-} ions arranged in a cubic close-packed arrangement in accordance with [20] in a regular pattern. The lattice parameter of the unit cell is $a = 0.839$ nm. There are eight crystal motifs per unit cell [21]. Its chemical formula can be described as $A[AB]O_4$, where $A = Fe^{3+}$, $B = Fe^{2+}$, and brackets indicate octahedral sites. In an inverse spinel structure, all the Fe^{2+} and half of the Fe^{3+} cations occupy octahedral sites and the remaining half of the trivalent iron occupy tetrahedral sites [22, 23]. The distribution of Fe^{3+} cations at the tetrahedral sites suggests the degree of disorder λ in the spinel structure, and the value of λ for an inverse spinel is $\lambda = 1/2$. Figure 2.2 shows the order of the Fe and O layers along the (001) direction.

The Fe^{2+} cations can be substituted with other metal cations, which produce different types of metal ferrites, such as $CoFe_2O_4$, $MnFe_2O_4$, $ZnFe_2O_4$, and $NiFe_2O_4$. The substituting ions are adjusted by the expansion or contraction of the oxygen framework to compensate the size difference from Fe^{2+} [25–28].

2.2.1.2 Maghemite γ-Fe_2O_3

Maghemite nanoparticles are broadly applicable in biomedicine owing to their excellent magnetic properties. At the same time, they can be made biocompatible and produce low toxicity [29, 30]. Maghemite occurs in nature as a weathering product of structurally related magnetite. The iron oxide γ-Fe_2O_3 is typically described both in a cubic system (space group $P4_3$ 32) with disordered Fe vacancy or in a tetragonal system (space group $P4_12_12$) with full site ordering and $c/a \approx 3$. Magnetite and maghemite have a similar spinel crystalline structure and, hence, identical electron diffraction patterns. Nevertheless, the latter have both Fe^{3+} and Fe^{2+}

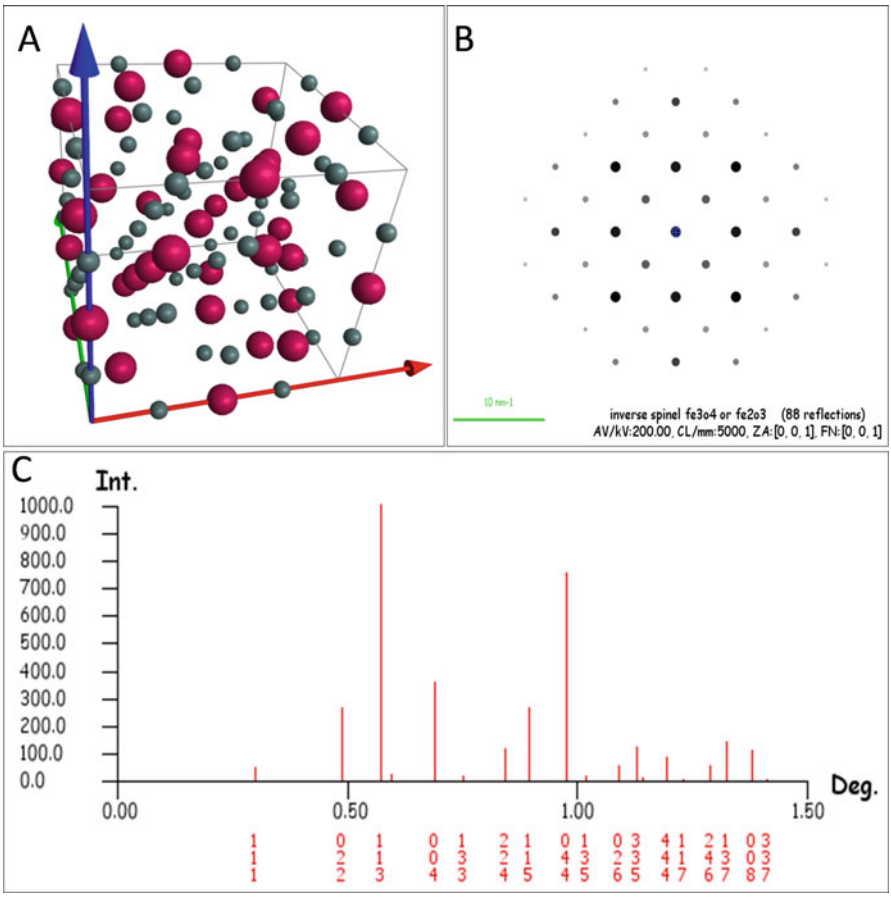

Fig. 2.2 Atomic structure and diffraction of inverse spinel magnetite simulated with JEM software [24]: (**a**) 3-D crystal structure along [001] zone axis (*gray spheres* oxygen atoms, *purple spheres* iron atoms). (**b**) Diffraction pattern oriented along [001] zone axis. (**c**) Powder electron diffraction pattern of inverse spinel magnetite or maghemite (angle described in powder electron diffraction is 2θ). The indexes of the diffraction peaks are given in *red*. (Note that chemically disordered maghemite would exhibit the same diffraction patterns as **b** and **c**; see next section). Space group: Fd3m. Atomic positions: Fe_1: 0.125, 0.125, 0.125; Fe_2: 0.5, 0.5, 0.5; O: 0.254, 0.254, 0.254. Lattice parameters: $a = 0.839$ nm

cations, whereas in maghemite, all the iron ions are in the trivalent state. The charge neutrality of the unit cell is compensated by the existence of cation vacancies. The cubic form of maghemite has a lattice parameter, $a = 0.834$ nm. Each unit cell of maghemite contains 32 oxygen ions, 21 1/3 ferric ions, and 2 1/3 vacancies. Eight Fe ions are located in the tetrahedral sites, and the remaining is randomly distributed over the octahedral sites, whereas vacancies occupy only the octahedral sites. Thus,

maghemite's chemical formula can be changed to A [AΔ] O_3, where A = Fe^{3+}, Δ = vacancies, and brackets indicate octahedral sites [31]. This structure can also be described using the Fd3m cubic space group.

The character and extent of arranging iron vacancies in octahedral sites have been studied by researchers for many years. Vacancy ordering depends on the nature of the precursor, the size of the crystallite, and the amount of iron ions in the structure. The space group Fd3m suggests a random distribution of cation vacancies over octahedral sites like magnetite, but vacancy ordering with 2 2/3 vacancies per unit cell is not permissible owing to the fractional number of vacancies. Thus, it is necessary to extend the cell three times along *c*, which ends in a tetragonal space group ($P4_12_12$), giving a formula of $Fe^{3+}{}_{24}$ [$Fe^{3+}{}_4O_8$] O_{96}. The lattice parameters are $a = 0.833$ nm and $c = 2.501$ nm. Usually, the tetragonal maghemite is associated with an ordered form and the cubic with a disordered form, but cubic phases with vacancy ordering still exist [32]. Figure 2.3 shows the chemically ordered maghemite crystalline structure and diffraction pattern simulated by JEMS software. By comparing the simulated diffractions of Figs. 2.2 and 2.3, we can observe additional superstructure reflections in the diffraction of the chemically ordered maghemite structure (Fig. 2.3). This chemical order allows us to differentiate between maghemite and magnetite using electron diffraction on HRTEM.

In brief, maghemite contains cation vacancies, which may be ordered (tetragonal superstructure), partially ordered (cubic structure), or totally disordered with a high possibility of the vacancies being aggregated [33].

2.2.1.3 Hematite α-Fe_2O_3

Hematite has remarkable applications in the field of gas sensors, magnetic storage media, solar cells, water splitting, and environmental treatment due to its nontoxicity, biodegradability, low corrosion, and low processing expenses [34–38]. It also serves as a starting material for synthesizing maghemite and magnetite [39].

Hematite can be described in a hexagonal (rhombohedral) $R\bar{3}c$ space group. In hexagonal unit cells, the lattice parameters are $a = 0.5034$ nm and $c = 1.375$ nm. The number of crystal motifs per unit cell is six. For hexagonal symmetry, the Miller index is (hkil), where it is usually equal to $-(h+k)$.

The crystallographic structure of hematite is similar to α-Al_2O_3, corundum. The anions form a hexagonal close-packed structure differentiated by the regular successive change in two layers; the atoms in both layers occupy the vertices of a sequence of equilateral triangles, and the atoms in one layer are located directly over the centers of the triangles in the neighboring layers. The cations occupy two-thirds of the octahedral sites [21]. In other words, the oxygen ions occupy hexagonal sites and the Fe cations are located only in the adjacent octahedral sites, though the six adjacent neighboring oxygen ions of an iron ion are slightly misaligned. Moreover, the four iron ions around each oxygen ion are not arranged in a regular

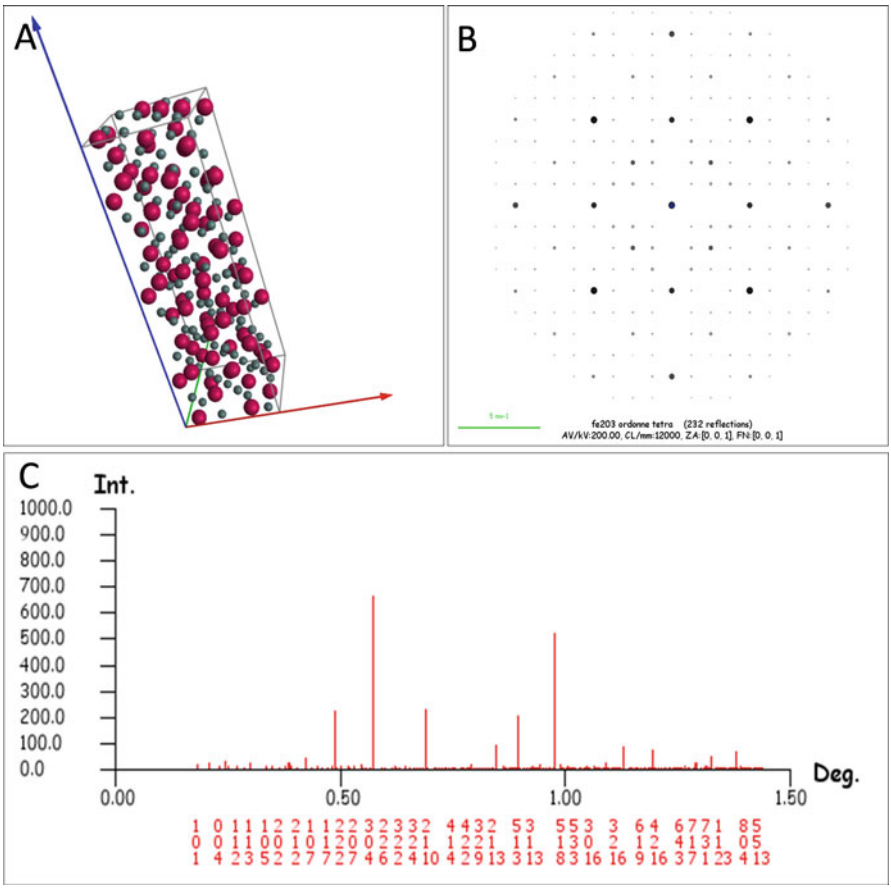

Fig. 2.3 Atomic structure and diffraction of chemically ordered maghemite simulated with JEMS for chemically ordered maghemite [24]: (**a**) 3-D crystalline structure along [001] zone axis (*gray spheres* oxygen atoms, *purple spheres* iron atoms). (**b**) Diffraction pattern oriented along [001] zone axis. (**c**) Powder electron diffraction pattern of chemically ordered maghemite (angle described in powder electron diffraction is 2θ). The indexes of the diffraction peaks are given in *red*. Space group: $P4_12_12$. Atomic positions: **Fe**: (0.742, 0.992, 0.039), (0.2579, 0.0079, 0.2057), (0.492, 0.7579, 0.1224), (0.615, 0.615, 0), (0.385, 0.385, 0.166), (0.375, 0.135, 0.08), (0.865, 0.625, 0.0867), (0.875, 0.365, 0.003), (0.125, 0.125, 0) and **O**: (0.611, 0.861, −0.0047), (0.361, 0.889, 0.0787), (0.389, 0.139, 0.162), (0.122, 0.377, 0.0003), (0.877, 0.378, 0.0837), (0.878, 0.623, 0.166), (0.374, 0.628, 0.0007), (0.128, 0.126, 0.084), (0.626, 0.372, 0.1673), (0.373, 0.376, 0.0843), (0.624, 0.627, 0.0843), (0.124, 0.873, 0.001). Lattice parameters: $a = 0.83$ nm, $c = 2.501$ nm

tetrahedron [40]. Figure 2.4 shows a 3-D view of the structure of hematite consisting of hcp arrays of oxygen ions placed along the [001] direction; Fe^{3+} occupy two-thirds of the sites, arranged in a regular pattern, with two filled sites accompanied by one unoccupied site in the (001) plane.

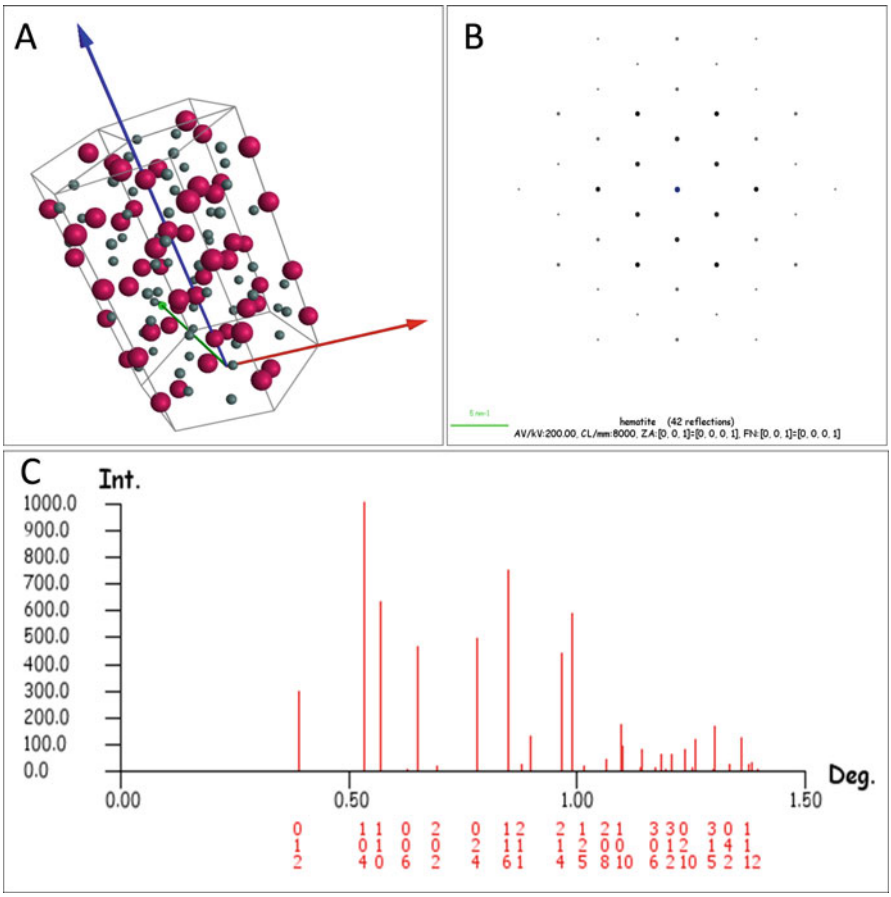

Fig. 2.4 Atomic structure and diffraction of hematite simulated with JEMS [24]: (**a**) 3-D crystalline structure along [001] zone axis (*gray spheres* oxygen atoms, *purple spheres* iron atoms). (**b**) Diffraction pattern oriented along [001] zone axis. (**c**) Powder electron diffraction pattern of hematite (angle described in the powder electron diffraction is 2θ). The indexes of the diffraction peaks are given in *red*. Space group: $R\bar{3}c$. Atomic positions: Fe: 0, 0, 0.3553 and O: 0.3059, 0, 0.25. Lattice parameters: $a = 0.503$ nm, $c = 1.375$ nm

2.2.1.4 Ferrihydrite

Ferrihydrite (Fh) is an extensive hydrous ferric oxyhydroxide mineral present on the Earth's surface [41, 42]. It has been reported that ferrihydrite also occurs in the core of the ferritin protein in living entities and serves to store excess iron [43]. Although we have not observed ferrihydrite in ferritins of ex vivo mice samples, we discuss the structure of ferrihydrite here. Ferrihydrite is a poorly crystalline iron oxyhydroxide. It has an estimated composition of $5Fe_2O_3.9H_2O$, although the actual formula for ferrihydrite is still not established owing to a lack of accurate knowledge of its water

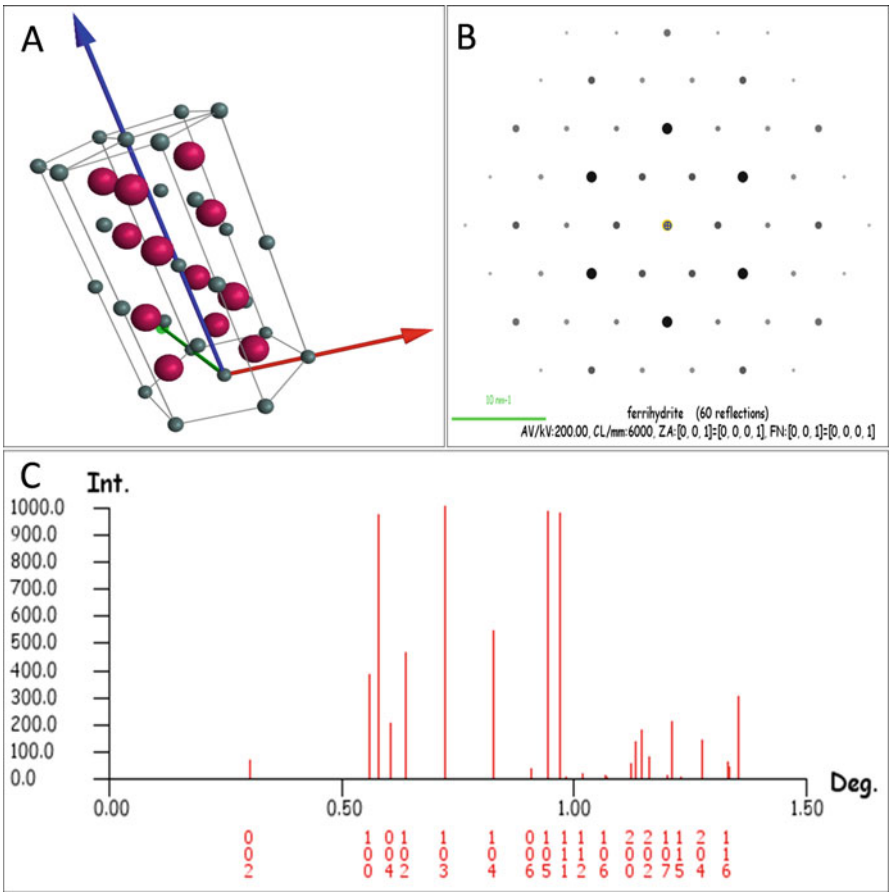

Fig. 2.5 Atomic structure and diffraction of ferrihydrite simulated with JEMS [24]: (**a**) 3-D crystalline structure along [001] zone axis (*gray spheres* oxygen atoms, *purple spheres* iron atoms). (**b**) Diffraction pattern oriented along [001] zone axis. (**c**) Powder electron diffraction pattern of ferrihydrite (angle described in the powder electron diffraction is 2θ). The indexes of the diffraction peaks are given in *red*. Space group: P31c. Atomic positions: Fe: 0.333, 0.666, 0.136, O (OH): 0, 0, 0, and O (OH): 0.666, 0.333, 0.25. Lattice parameters: $a = 0.295$ nm, $c = 0.937$ nm

content. The degree of crystallinity of ferrihydrite is classified as two-line, four-line, and six-line ferrihydrite because it is well known that the number and width of X-ray diffraction (XRD) peaks are directly linked to crystallinity. Figure 2.5a shows the 3-D arrangement of atoms in ferrihydrite that has a hexagonal structure with unit cell parameters of $a = 0.296$ nm and $c = 0.949$ nm. The space group of this structure is P31c [21]. Figure 2.5b, c shows the diffraction pattern along the [001] direction and powder electron diffraction pattern obtained by JEM software [37], respectively.

2.2.1.5 Cobalt Ferrite (Cobalt Ferrite Nanoparticles)

Cobalt ferrites belong to the so-called hard ferrites and have many applications in the fields of medicine, permanent magnets, catalysts, microwave devices, and high-density information storage [44–47]. They are crystallized in an inverse spinel structure just like magnetite, except that divalent iron ions are replaced by cobalt ions [48]. As the ionic radii of divalent Fe and Co are the same, there is no change in the lattice parameter (i.e., $a = 0.839$ nm) of the unit cell.

2.3 Nucleation, Growth, and Arrested Growth

2.3.1 Introduction

The isolation of solid states from liquid phases is an ancient method, but currently it plays a key role in various industrial procedures. To attain the quality of fine products, for economic reasons and environmental effects, the optimization of this phase is necessary [49].

To attain this goal, various theoretical and experimental principles or procedures have been developed. In physical chemistry the following procedures are studied: solubility product, crystal growth, supersaturation, common ion effect, filtration, crystallization, heterogeneous and homogeneous nucleation, precipitation, and coprecipitation. In addition to the effects of pressure, temperature, and additives, the kinetic, thermodynamic, and statistical features of nucleation, precipitation, and crystallization are verified. Some significant methods, such as crystal growth and nucleation, are mostly used in different environments like alloys, vapor phases, interfaces, and glass matrices. The most common approach for the analysis of these methods is to develop a specific treatment. In the liquid phase, the main conditions for the appropriate precipitation procedure are purity and the recovery of the majority of the final product [9].

2.3.1.1 Thermodynamic Considerations

The thermodynamic stability of a substance A in a solution with respect to the pure crystalline solid phase depends on the difference ($\Delta\mu$) between the chemical potential (μA) of A in both phases:

$$\Delta\mu = \mu_{\mathrm{A,solid}} - \mu_{\mathrm{A,solution}} = RT \ln \frac{a_{\mathrm{A,sat.solution}}}{a_{\mathrm{A,solution}}}. \tag{2.6}$$

If Dμ < 0, then some portion of species A will develop a solid phase moving from the solution to the solid phase until Dμ = 0 and a dynamic equilibrium is established between A in both the solid and liquid phases. On the other hand,

if $D\mu > 0$, in saturated solution ($a_{A,sat\ solution}$), if the activity of A in the state of equilibrium with pure A is more than that in the actual solution ($a_{A,solution}$), the material will remain completely molecularly isolated in the liquid phase. Also, the system will be thermodynamically stable and have a single phase. Because of these main properties, $D\mu$ is also known as the driving force behind crystallization.

For sparingly soluble solutes, the driving force ($D\mu$) is associated with entropy (ΔS) and enthalpy (ΔH):

$$\Delta\mu = \Delta H - T\Delta S. \tag{2.7}$$

The preceding equation highlights the relationship between entropic and energetic terms used to control the factors of the crystallization method. Various thermodynamic equations are used to predict the pressure and temperature dependency of the driving force ($D\mu$) [50]. Also, when the activity coefficients in the liquid and solid phases are known, thermodynamics establishes the relationship between the driving force ($D\mu$) and the solubility of nonionic and ionic solutes [51].

2.3.1.2 Kinetic Considerations

Usually, above the solubility limit, crystallization or precipitation occurs rapidly in the presence of a solid phase established due to different substances (heterogeneous nucleation) or the same substance (secondary nucleation). The existence of a solid phase that interacts with the solution offers a surface on which molecules of species A could grow as well as nucleate [52, 53]. In this situation, the factors that control the rate of the entire procedure are (1) the nature and area of the solid phase exposed to the solution; (2) the appearance of the species on the surface of the solid phase and vice versa by mechanical agitation, thermal diffusion, or convection currents; and (3) the incorporation rate of the precursors to the crystal lattice [54, 55]. The incorporation phase contains the partial release of solvating species, the adsorption of a precursor, and a useful setup in the lattice. Usually, anisotropic morphologies are examined when fewer or more molecules are trapped in specific crystal faces.

In homogeneous nucleation, the creation of a solid phase cannot take place owing to the absence of a preexisting solid phase, and the liquid system will be stable kinetically [56–58]. The creation of a crystalline phase is not a single-step process; it is a multistep process that requires the strengthening of molecular groups of cumulative size according to the scheme

$$A_{N-1} + A \rightleftarrows A_N \tag{2.8}$$

or, in agglomeration processes,

$$A_i + A_j \rightleftarrows A_{i+j}. \tag{2.9}$$

At the molecular level, Brownian diffusion of species is a driving force behind these methods that allows their random occurrence. For this purpose, a thermodynamics property must be considered to know whether the solid phase will be established or not from ionic or molecular precursors. The free energy of formation of a nucleus comprised of N molecules, DG_f, given by

$$\Delta G_f = N\Delta_\mu + \Delta G_s. \tag{2.10}$$

The preceding equation is comprised of the term $N\Delta_\mu = \mathrm{NkT}\ \ln \frac{a_{\mathrm{A,sat.solution}}}{a_{\mathrm{A,solution}}}$, which includes the thermodynamic driving force for the growth of aggregate, and the other term ΔG_S is a result of the formation of a boundary between the surroundings and the aggregate. The last term of the preceding equation is given by

$$\Delta G_s = A_{N\gamma_s}, \tag{2.11}$$

where A_N represents the aggregate surface ($A_N = \mathrm{K_N N^{2/3}}$) and γ_s is the interfacial energy per unit surface.

According to the molecular approach, the interfacial energy ΔG_s determines the difference in the energetic state between the species situated in the interior and at the particle surface. This should be positive because at the surface, the energetic state of a species must be greater than that in bulk; then the boundary would be enhanced indefinitely [51].

If the molecules are at the surface or in a bulk, the time average of all the forces acting on them is zero. The strength and number of chemical bonds formed at the surface is smaller than that of bulk species. Embryos are thermodynamically unstable against abnormal growth.

Here, two states, such as bulk and surface species, have been considered. But it must be taken into account that when two phases interact with each other, an imprecise and interfacial domain is produced [54]. In a particle, this indicates the presence of more than two states of A. The first term for the supersaturated solutions ($\mathrm{a_{A,solution}} > \mathrm{a_{A,sat.solution}}$) will be negative, but the second term will always be positive. In these conditions, the dependency of such contributions and of ΔG_f on N is shown in Fig. 2.6.

The value of N^* corresponding to the maximum ΔG_f is known as the critical aggregation number. Aggregates with $N > N^*$ are known as nuclei; they grow naturally because a decrease in free energy increases their size. Aggregates with $N < N^*$ are known as embryos; they decompose because a decrease in the system free energy decreases N.

2.3.2 Growth Mechanism and Size Control

According to kinetic and thermodynamics properties, above the supersaturation threshold, the boundless growth of a nanoparticle is a natural process, and the growth rate can be managed by changing some factors such as temperature,

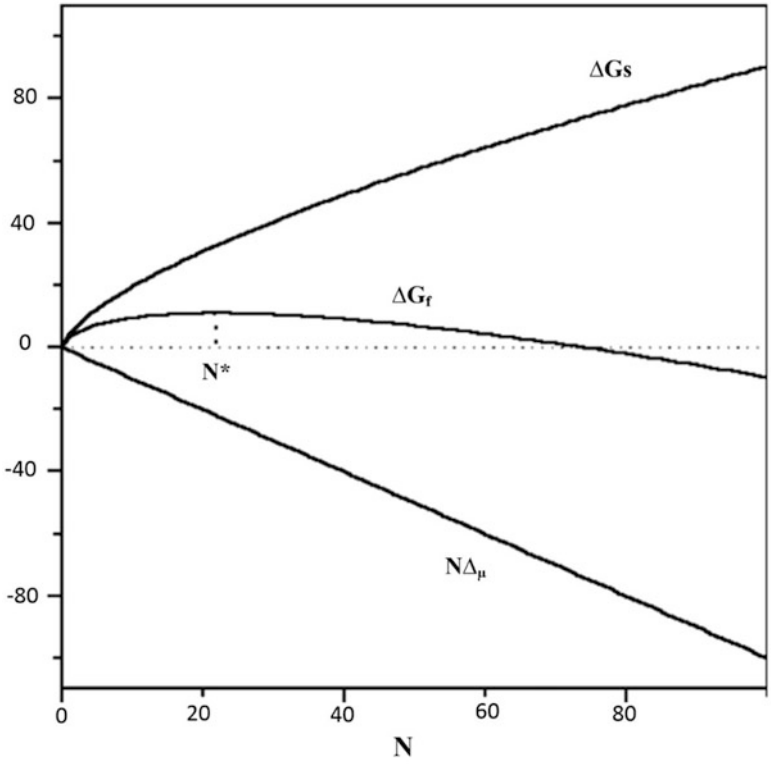

Fig. 2.6 N dependence of free energy of formation of a nucleus (ΔG_f), bulk crystal ($N\Delta_\mu$), and interface (ΔG_S). Figure reprinted/adapted with permission from [51]

supersaturation degree, and additive presence. To place a constraint on this process, other phenomena must play a role. The proper use of these parameters can lead to thermodynamic or kinetic refined nanoparticles of a controlled size [59]. The important types will be further discussed in the following subsections.

2.3.2.1 Nanoparticle Size Dependence on Time

In supersaturated solutions, the possibility of critical aggregate formation is very important in homogeneous conditions. There are three different methods that describe crystal growth, competitive and normal growth and nucleation. Moreover, other processes occur, such as aggregation, crystal growth, agglomeration, recrystallization, nucleation, time aging, induction time, solid-phase transitions, and amount of solid phase. Overlapping zones occur because not all phases are well isolated in time [60–62].

When the concentration of precursor becomes negligibly small, competitive growth controls the whole process. During this step, a movement of mass from minute particles to bigger particles takes place, and the following equation describes the time dependency of a cluster size:

$$\bar{r} \propto t^{0.33}. \tag{2.12}$$

It must be pointed out that the preceding equation represents the tendency toward an indefinite growth of crystal size. Mostly, when the size of a particle attains a system-acquired value as a result of the association of smaller aggregates or a growing process, it manages to isolate from the liquid state under the influence of the gravitational force that arises owing to Brownian movements.

In these conditions, a lower or upper solid phase depending on the bulk medium and the density of particles is developed. From homogeneous solutions, the precipitation of scarcely soluble materials results in an extensive particle size distribution owing to the random growth of a crystal [63]. After precipitation, various secondary processes can take place, such as aging, recrystallization, and aggregation. These processes involve additional changes in the structure, size, effectivity, and shape of crystals [64].

2.3.2.2 MNP Growth Inhibition and Size Control

In some situations, the growth of a particle is due to the existence of some other phenomenon. Various physicochemical methods allow one to control the size of nanoparticles:

- Passivation of nanoparticle surface by adsorption of suitable species,
- Charging of nanoparticles,
- Compartmentalization of nanoparticles in different zones.

Every mechanism has its own uniqueness and drawbacks that must be considered when selecting a synthesis process [65]. The stability of particles is due to the presence of a net charge and the establishment of an electric double layer surrounding the particle. In polar solvents, this is a very common phenomenon because the particle can adsorb ionic species of the solution, or species placed on the particle surface can separate, emitting ions to the adjacent medium. A double layer that surrounds the particle is generated by these methods along with an electrostatic effect on other neighboring ionic species. Owing to electrostatic forces, particles having similar charges or bounded by an electrical double layer repel each other. In such circumstances, when the particle–particle repulsive force overcomes attractive forces, such as hydrogen bonding and van der Waals forces, a stable scattering takes place. Electrostatic stabilization is powerfully reactive in the presence of electrolyte solution, to their charge and concentration, and at relatively low concentrations of nanoparticles, stable scattering can occur [66]. In particular, two contradictory results can be observed: ions resulting from electrolyte

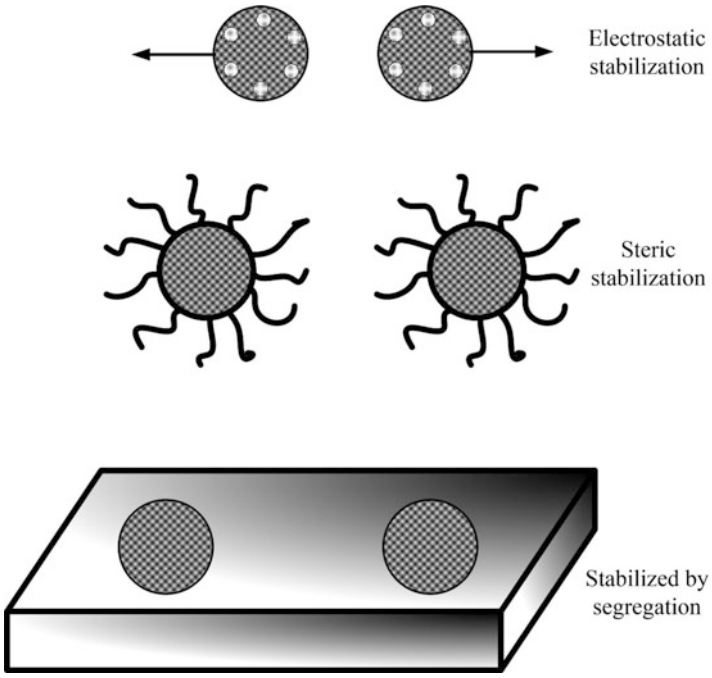

Fig. 2.7 Mechanisms allowing nanoparticle size stabilization. Figure reprinted/adapted with permission from [68]

dissociation can be selectively adsorbed, creating a charge on the surface of a nanoparticle or neutralizing preexisting charges. It must be taken into account that when two particles come into contact with each other, the charge distribution around each particle is changed as a result of the charge mobility on the particle surface, electrostatic forces, or the charged double layer coating the particles (Fig. 2.7). The subsequent charge distribution involves a reduction in the repulsive forces, so the particles will be able to approach each other and other distance dependent interactions can play their role. In addition, other attractive forces, for example, capillary forces and chemical bonds, can become effective at small distances [67]. For instance, it has been observed that negatively charged silica particles are easily deposited in the presence of negatively charged polymer latexes [68].

The double layer electrostatic repulsion and the presence of a net charge on the surface can regulate the stability of particle diffusion in polar and aqueous media [69, 70]. Some particular mechanisms, like proton exchange between surrounding medium and particle surface, are used to sustain surface charges in solvents with small dielectric constants [71]. Particles can also be stabilized by the deliberate use of suitable capping agents. From a molecular approach, molecules that show a chemical or physical affinity for species located at the surface of nanoparticles and form a shielding layer that makes the nanoparticle surface unreactive against

precursor incorporation and agglomeration are known as capping agents. The action of capping agents depends on their particular structure. In particular, they have an unreactive moiety attracted toward the environment and another type of molecular moiety exhibiting an affinity for the surface of nanoparticles. In the presence of unreactive additives or electrolytes, stabilization achieved through surface capping is usually not responsive. For nanoparticles, capping with chemically bonded species may serve as a catalyst.

In different domains, particles can be stabilized against abnormal growth by compartmentalization or segregation. This approach depends on the material exchange method and the inhibition of nanoparticle encounters. This strategy can be attained by scattering particles in a solid matrix or chemically attaching them to the surface of an appropriate substrate. In these situations, particle growth can be avoided by suspending diffusive methods. In various applications (catalysis or optical), this strategy has been extensively used in the preparation of nanoparticles.

Owing to the synthesis of nanoparticles in microheterogeneous systems, a stable-sized nanoparticle can be attained. Compared to the aforementioned mechanisms, this approach has unique characteristics. The formation of nanoparticles takes place in two steps: (1) slow growth of nuclei and (2) fast growth. At high concentrations, separation is obvious [72, 73].

In microheterogeneous systems, specific stabilization mechanisms are observed. Such microheterogeneous systems are used to stabilize nanoparticles. The nanoscopic domains of microhetrogeneous systems serve as a physical border that prevents nanoparticles and precursor diffusion, agglomeration, and encounters. In homogeneous media, the rate of formation of nanoparticles is generally faster than in microheterogeneous systems. This is similar to what is observed in biological systems, such as liposomes or biological membranes.

When a collection of molecules is restricted in a nano-sized area, some additional factors that play a role in the stability of the system could originate from the following sources:

1. Owing to the adsorption on the aggregate surface of a monolayer of surfactant molecules, the particle interfacial energy changes. It must be determined whether the aggregate surface is lipophilic or hydrophilic, as this feature controls the alignment of micellar aggregate or surfactant on the particle surface. If a nanoparticle is isolated in water, a subsequent layer of surfactant molecules is usually created, coating the primary layer and creating a bilayer surrounding the particle, and the surface is known as hydrophilic [74].
2. The encounter frequency decreases owing to the screening effect of the surfactant layer on internanoparticle attractive interactions and to the diffusion of micelles in the solvent medium.
3. A significant reduction in the particle growing process owing to the drastic decrease of the diffusion rate provides sufficient time for various other processes, for example, particle coating with a special type of molecule allowing for stabilization and regulation of small-sized particles.

4. Inhibition of heterogeneous nucleation occurs owing to the coating effect of a monolayer of surfactant molecules on particles or possible solid surfaces in the system.
5. An adjustment takes place in the microscopic processes that make it possible to control the growth and formation of nanoparticles.
6. Thermodynamic and kinetic factors vary in confined spaces.

2.3.3 Novel Synthesis Methods for Size-Controlled MNPs

Spinel ferrites have remarkable magnetic and electrical properties. The sintering and synthesis of ferrites is considered a powerful technique in current ceramic research, and spinel ferrites have notable applications. Because of their low coercivity and high resistance, spinel ferrites have been extensively used in transformers and microwave appliances. The spinel structure is based on a fcc arrangement of oxygen atoms with the stuffing of cations in either octahedral or tetrahedral spaces within this arrangement; in a unit cell 8 out of 64 tetrahedral sites and 16 out of 32 octahedral sites are occupied. These kinds of compounds have both inverse and normal spinel structures. For a normal spinel structure, the octahedral holes are filled by Fe^{3+} ions and the tetrahedral holes are occupied by transition metal ions [75]. In an inverse spinel structure, half the Fe ions pack all the tetrahedral sites and the transition metal ions and the other half of the Fe ions fill all the octahedral sites.

Various chemical methods applied to synthesize magnetic nanoparticles (MNPs) have been presented [76], including the polyol method [77], flow injection synthesis [78], and electrochemical techniques [79, 80]. Because of the colloidal nature of superparamagnetic nanoparticles, it is difficult to synthesize them [60]. Comprehensive studies on the synthesis of small MNPs with well-defined shapes have been conducted by many researchers [21, 81].

2.3.3.1 Classical Synthesis by Coprecipitation

In chemical routes of preparation of nanoparticles with preferred physical properties, the structural and chemical properties of the elements also play an important role. Fine chemical homogeneity can be attained by mixing constituents at the molecular level. Moreover, this makes it possible to control the shape and size distribution during synthesis. Chemical methods of preparation have emerged as an important technique and are used for the synthesis of spinel ferrite nanoparticles [82].

The coprecipitation process is the most proficient technique used for the synthesis of MNPs. This technique involves mixing ferrous and ferric ions in a molar ratio of 1:2 in a solution at room temperature or higher. The formation of ferric oxide can be achieved under the following chemical reaction:

$$Fe^{2+} + 2Fe^{3+} + 8OH^- \rightleftarrows Fe(OH)_2 + 2Fe(OH)_3 \rightarrow Fe_3O_4 + 4H_2O. \quad (2.13)$$

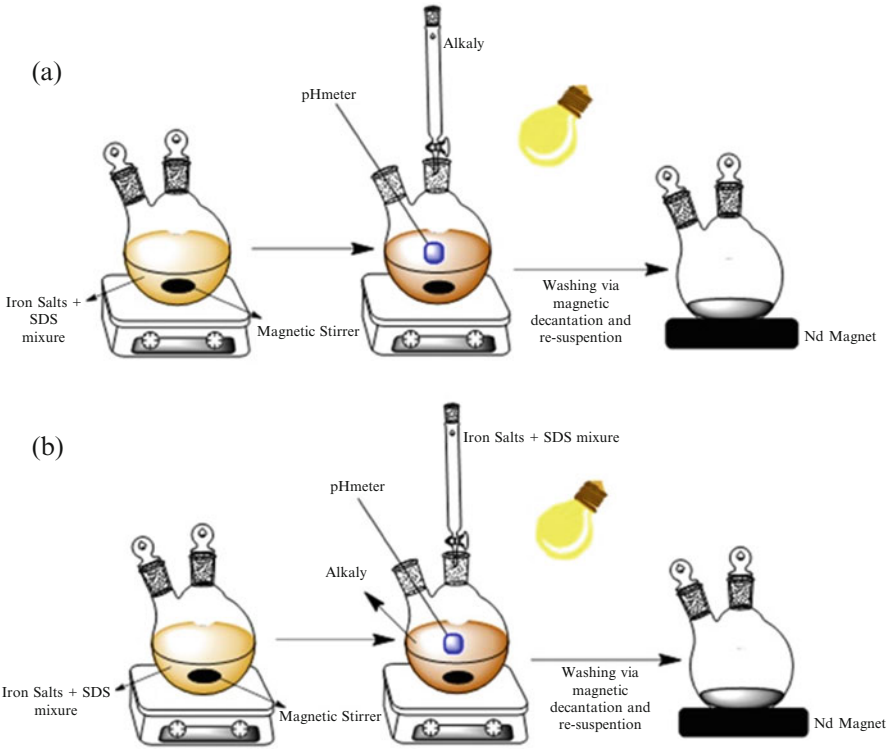

Fig. 2.8 Coprecipitation method. (**a**) Traditional synthesis. (**b**) Inverted synthesis. MNPs synthesized by coprecipitation and modified with sodium dodecyl sulfate (SDS) in a postsynthesis step. Inverted coprecipitation was carried out by adding the Fe^{2+}/Fe^{3+} aqueous solution containing the proper amount of SDS to the alkali solution. Figure reprinted/adapted with permission from [86]

The reaction is controlled by changing the solution pH. The growth of a ferric oxide nucleus is comparatively simple when the pH of the solution is greater than 11, while the nucleation of a ferric oxide nucleus is comparatively simple when the solution pH is less than 11 [83]. Coprecipitation has been examined mostly in the preparation of ferric oxide nanoparticles because of its ease of use in gram-scale fabrication (Fig. 2.8) [84]. Many researchers have reported the extensive coprecipitation synthesis of ferric oxide nanoparticles, where their magnetic properties and morphology at various different temperatures were examined [85]. Various modified coprecipitation processes have been developed. Many researchers have reviewed the advancements and developments in this field over the last decade [83]. In the presence of oxygen, magnetite (Fe_3O_4) oxidizes and converts to maghemite:

$$Fe_3O_4 + 2H^+ \rightarrow \gamma\text{-}Fe_2O_3 + Fe^{2+} + H_2O. \tag{2.14}$$

This equation shows that iron ions are desorbed from the Fe_3O_4 surface, producing cationic holes and forming γ-Fe_2O_3. Hence, the oxidation of Fe_3O_4 involves the oxidation–reduction of the surface of magnetite (Fe_3O_4). Maghemite and magnetite differ from each other in terms of the distribution of iron ions in the tetrahedral and octahedral sites of the spinel structure [79].

In an octahedral site, maghemite (γ-Fe_2O_3) has cationic holes. The ordering of vacancies is related to the synthesis process, which results in symmetry lowering and perhaps superstructures. The vacancies may be partially or completely random or absolutely well arranged. According to the results of XRD and Fourier transform infrared (FTIR) spectroscopy, vacancy ordering occurs only for particles greater than 5 nm in size [87].

The coprecipitation method is used for the fabrication of nanoparticles on a large scale. However, kinetic factors control only the crystal growth while the particle size distribution cannot be definitively measured. The mechanism of this process can be described by the two phases [88, 89]; First, when the concentration of reactant approaches critical supersaturation, an initial short nucleation occurs. Second, due to the dispersion of solutes to the crystal's surface, regular growth of nuclei takes place. Several parameters are used to control the surface and magnetic properties, shape, and size of iron oxide nanoparticles (IONPs). By varying the temperature, pH, Fe^{2+}/Fe^{3+} ratio, and ionic strength, the shape and size of IONPs can be modified [79].

Many researchers have examined the effect of the main parameters on the production of IONPs using the coprecipitation technique. For instance, in [90] the effect of the Fe^{2+}/Fe^{3+} ratio on the magnetic properties, size, and morphology of coprecipitated nanoparticles is discussed.

The effect of iron concentration and iron media have been examined [91]. The Fe^{2+}/Fe^{3+} ratio is the main parameter used to attain the desirable yield and size of IONPs during synthesis. Increasing the Fe^{2+}/Fe^{3+} ratio reduces the preparation yield and enhances the mean particle size.

Moreover, the ionic strength and acidity of the precipitation agent are the main factors on which the mean size of magnetic nanoparticles depends [92]. Narrow particle size distribution and small particle size can be attained under elevated ionic strength [93].

Biocompatibility and aggregation are major hindrances in biomedical applications of IONPs. In the coprecipitation process, various biomolecules and surfactants are directly inserted. The coprecipitation technique is one of the most established and effective techniques used in the synthesis of IONPs with high saturation magnetization, and to overcome the limitations of this technique more attention should be devoted, for instance, to the use of a strong base in reactions and a wide particle size distribution [83].

2.3.3.2 Synthesis by Hydrothermal Method

The hydrothermal method is one of the well-known techniques that have attracted scientific community for nanomaterial synthesis. This is due to its simple and easy synthesis mechanisms. This technique is economical and highly efficient and has potential for large-scale production. In general, the hydrothermal method uses an aqueous medium in a reaction reactor under high temperature and pressure. The size and shape of the particles can be accurately controlled by adjusting the synthesis parameters such as temperature, pressure, reaction time, concentrations and ratio of reactants, type of solvent, and reaction path. In the hydrothermal method, the size of the particle is usually controlled by the crystal growth and rate of nucleation [94]. Generally, nanomaterials synthesized by the hydrothermal method do not need further calcination at high temperatures, which minimizes the risk of nanomaterial reclustering. The hydrothermal method can be used to synthesize a wide range of nanostructured materials [95, 96]. A generalized hydrothermal method for various types of nanomaterial synthesis can be explained as shown in Fig. 2.9.

Magnetic nanoparticles have also been synthesized using the hydrothermal technique. In this regard, octahedral $NiFe_2O_4$ ferrites were synthesized by hydrothermal reaction under mild conditions. FTIR spectroscopy and XRD were employed for constitution measurements and composition of these ferrites. Morphological measurements were done by scanning electron microscopy and these were found octahedral in morphology having mean particle size of ca 40 nm. Crystallite size from XRD analysis was obtained as 39 nm, which is in good agreement with

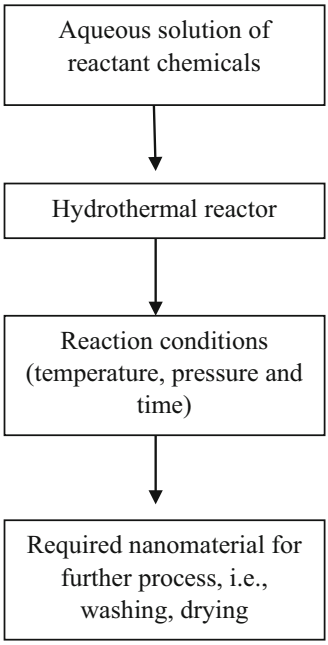

Fig. 2.9 Generalized hydrothermal method for various types of nanomaterial synthesis. Reproduced with permission from [96]

scanning electron microscopy (SEM) results. Electron diffraction and consequent transmission electron microscopy studies confirmed the single crystalline nature and morphology of the octahedral nanoparticles. Magnetic behavior was also investigated, and it was shown that $NiFe_2O_4$ octahedrons had the same coercivity because of the lower morphological anisotropy [97]. TEM investigations revealed that cobalt oxide nanorods have a nanoporous structure, involving the aggregations of nanorods. Magnetic properties indicate that cobalt oxide nanorods have a lower Ne transition temperature, around 35 K. The optical properties of cobalt oxide nanorods were investigated by ultraviolet-visible and Raman spectroscopy [98].

Various properties of cobalt ferrite ($CoFe_2O_4$) nanoparticles have been examined. The hydrothermal technique via a polyethylene glycol (PEG) was used for the synthesis of cobalt ferrite nanoparticles. TEM and XRD analysis were used to investigate the morphological, structural properties of the prepared nanoparticles, and a vibrating sample magnetometer (VSM) was used to examine the magnetic properties. The formation of a pure spinel phase was verified by XRD analysis and the crystallite size was in the range of 10.0–32.0 nm. An increase in the average size of the cobalt ferrite ($CoFe_2O_4$) nanoparticles was also reported as the hydrothermal temperature increased. The size and morphology of the nanoparticles were affected by the hydrothermal temperature, and the morphology of the cobalt ferrite ($CoFe_2O_4$) nanoparticles transformed into an octahedral from a spherical shape as the hydrothermal temperature increased. The characterization of the magnetic properties showed that the coercivities and saturation magnetization of the synthesized cobalt ferrite ($CoFe_2O_4$) nanoparticles become enhanced as the mean size of the cobalt ferrite ($CoFe_2O_4$) nanoparticles increases [99].

Nanoparticles of magnetite (Fe_3O_4) were synthesized using the hydrothermal technique. A contrast agent was used in these nanoparticles to study their applications in MRI. Ferric chloride ($FeCl_3$) and ferrous chloride tetrahydrate ($FeCl_2.4H_2O$) were used as precursors, with sodium hydroxide as reducing agent to start the precipitation of magnetite (Fe_3O_4). Then a layer of chitosan (CHIT) was deposited on the surface of the magnetite's (Fe_3O_4) nanoparticles to increase its biocompatibility and stability. TEM was used to investigate the size distribution of the prepared magnetite (Fe_3O_4) nanoparticles. XRD analysis confirmed the formation of a cubic inverse spinel structure of magnetite (Fe_3O_4) nanoparticles. The FTIR spectrum showed the presence of CHIT on the surface of the synthesized magnetite. The magnetic properties of the magnetite nanoparticles were characterized using a VSM at room temperature. A customized phantom study of MRI proved that the Fe_3O_4 nanoparticles showed better results as contrast agent [100].

The cause of the inhibition of the surfactant was studied for $NiFeO_4$ nanoparticles prepared by the hydrothermal method. The sample was prepared in the presence of sodium dodecyl sulfate and glycerol. XRD, inductively coupled plasma atomic emission spectrometer (ICP-AES), transmission electron microscopy (TEM), and vibrating sample magnetometer (VSM) techniques were employed to investigate the specimens. The crystallinity was increased by increasing the temperature.

In the presence of surfactants, the crystallinity of the $NiFe_2O_4$ nanoparticles was decreased. Furthermore, all of the ferrite nanoparticles were highly paramagnetic at room temperature [101].

2.3.3.3 Polyol Method

Currently, the polyol method has become a preferred technique in the preparation of uniform MNPs. The polyol technique is widely used at high levels of biomedical applications as a tool of investigation; for example, MRI is a polyol technique [102]. Polyols [e.g., ethylene glycol (EG), diethylene glycol (DEG)] are used to reduce metal salts to small-sized metal particles [103]. This process has been used for the production of inorganic compounds [104]. The polyol method was first used for the preparation of noble metals (Pt, Ru, and Au) and other metals like cobalt (Co), copper (Cu), and nickel (Ni) [105, 106]. Nowadays, this synthesis method is being used to synthesize several metals, such as iron-based alloys [107], that can be used in various applications such as in biomedicine.

The polyol method [108] is similar to a sol-gel process. In a sol-gel process, an oxidation reaction is involved, but in the polyol method, a reduction reaction is involved [60], and such a reduction reaction is useful for the synthesis of both microparticles and nanoparticles with well-described shapes and a narrow range of sizes [109]. Polyols such as PEG possess some remarkable properties. They serve as solvents owing to their relatively high dielectric constant and their high boiling point (BP), they occur in a wide temperature range (25 °C to BP) for the preparation of inorganic mixtures [110].

Polyols do not just act as solvents and reducing agents but also serve as stabilizers to manage particle sizes and are used to prevent particle accumulation. In the polyol synthesis method, a metal precursor mixture is suspended in a liquid polyol. First, the suspension is stirred and then heated to a relatively high temperature; this temperature should be as high as the BP of polyols [60, 111]. The narrow size and well-defined shape of nonagglomerated metal nanoparticles can be attained by controlling the kinetics of precipitation [102]. By raising the temperature of reaction or inducing heterogeneous nucleation, some particles, like those of submicrometer-size, can be synthesized. Iron nanoparticles can also be obtained by disproportionation of $Fe(OH)_2$ in organic medium [108].

Recently, Cai and Wan [104] presented a simple process by modifying the polyol process to directly attain nonaggregated MNPs. [104]. The four major kinds of polyols are ethylene glycol (EG), diethylene glycol, triethylene glycol, and tetraethylene glycol [104, 111]. Cuboid iron-manganese oxide nanoparticles with unprecedented dimensions as large as 33 ± 5 nm (average body-centered diagonal) were obtained in monodisperse form by varying the ester content. The shape and size of these unusually large MNPs can be controlled simply by varying the surfactant composition, leading to increased control over the dimensions of the nanoparticles (Fig. 2.10).

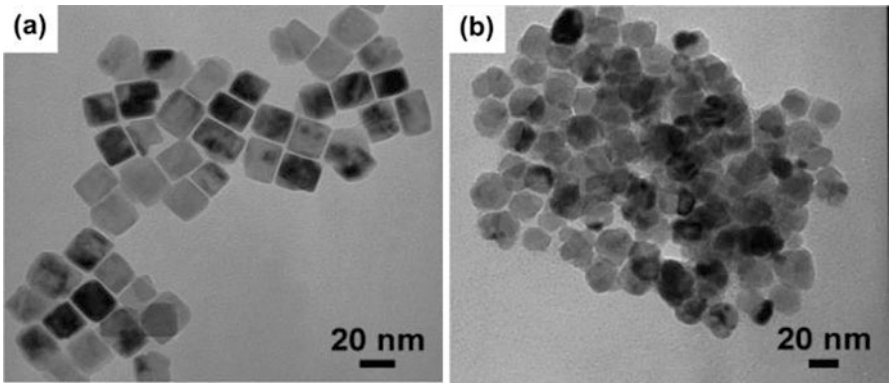

Fig. 2.10 Shape variation of iron-manganese oxide nanoparticles. Figure reprinted/adapted with permission from [20]

Only the reaction with triethylene glycol produced nonagglomerated MNPs of small size and uniform shape (Fig. 2.9). This result shows that the polyol solvent performs a vital role in determining the colloidal stability and morphology of the obtained particles [104]. The occurrence of polyol ligands on the surface of MNPs can be confirmed by FTIR spectroscopy analysis [60]. When sodium hydroxide (NaOH) and Fe (II) chloride reacts with EG, precipitation arises at a low temperature of 80–100 °C [102].

2.3.3.4 Electrochemical Method

The electrochemical process has been used extensively to prepare different phases of iron oxide nanoparticles like Fe_3O_4 or γ-Fe_2O_3 [58]. In this process, a current is passed through a cathode and anode placed in an electrolyte. In an electrolyte, the anode can be oxidized into a metal ion and the cathode can then be reduced to a metal in the presence of stabilizers. At the electrode–electrolyte boundary, synthesis occurs. The electrosynthesis process has various specific characteristics. The electrochemical process occurs near the electrode with a relatively high potential gradient (105 Vcm^{-1}) [79]. Under these conditions, the reactions form products that cannot be obtained using other techniques. The product formed in this reaction is deposited on an electrode, known as a thin film. If a properly shaped electrode is immersed in an electrolyte, a uniform polarization is acquired. The temperature should be moderate and not be as high as the BP of the electrode [79]. The electrochemical process relies on both oxidation and reduction reactions; by changing and regulating the cell potential, the power of both oxidization and reduction can be selected and regularly altered. This unique characteristic cannot be achieved by other synthesis methods. The structure of the thin film or coating can be measured by altering the bath composition [79]. However, this technique

has some limitations, for example, all reactions take place at room temperature, and the electrosynthesis process forms rough products. X-ray characterization of synthesized products formed in this process reveals amorphous impurities [79].

The electrochemical synthesis of maghemite nanoparticles was carried out in an organic medium. Using this method, 3–8 nm γ-Fe_2O_3 particles were prepared from an Fe electrode in a liquid medium of a cationic surfactant [58, 112]. The size of maghemite (γ-Fe_2O_3) nanoparticles can be adjusted by the current density [102]. Under oxidizing conditions, electrochemical deposition has been used for the production of Fe_2O_3 and Fe_3O_4 nanoparticles [113].

In this method, the particle size can be managed by changing the current density or potential. Moreover, it is possible to avoid the aggregation of magnetic nanoparticles if the synthesis is carried out in the presence of surfactants [80]. Some work has been done in this field. Using a conventional process, a size of 20 or 30 nm of Fe_3O_4 nanoparticle is difficult to obtain. The electrochemical synthesis of magnetite (Fe_3O_4) is carried out in an aqueous solution [80]. The particles generated in this process are hydrophobic, and the surface of these particles can easily be changed by an exchange reaction with specific biomolecules. Various techniques, such as TEM, IR spectroscopy, and XRD, have been used mostly for the characterization of generated nanoparticles [80].

2.3.3.5 Flow Injection Technique

The flow injection synthesis (FIS) technique is an adapted form of the coprecipitation process [83]. In various "matrices" like emulsion, the reaction zone confinement is mostly utilized to obtain small nanoparticles. Moreover, a particular pattern of a device can serve as a substitute for the "matrix" confinement [60, 114]. The synthesis of MNPs depends on the flow injection synthesis method. This method is comprised of segmented or continuous mixing of substances in a capillary vessel. In the reaction, various precursors can be inserted by injecting an adjustable amount of flow. Flow injection synthesis has some advantages, for example, high mixing homogeneity and reproducibility. Alvarez studied the impact of chemical factors on the characteristics of various materials [115]. MNPs with a size of 2–7 nm can be obtained in this process [60, 116].

2.4 Strategies to Control the Size and Shape

The morphology and size control of nanoparticles is an important topic for researchers and represents a challenge [117–119]. This topic has further specified applications that might be used more proficiently in different areas. For example, different in vivo properties have been detected using needle or spherically shaped MNPs [120]. Likewise at the cellular level, it seems essential to know MNPs' surface charge for interpreting their uptake capability [121].

Using expensive, complex, and energy-intensive procedures like the acetyl acetanoate of Fe, a polyol, the preparation of identical and nearly individual MNPs can be achieved; however, coprecipitation is proposed when a low-cost, non-time-consuming, and simple method is desired. This popular method includes aqueous salt solutions of iron (Fe^{2+}/Fe^{3+}) and a base used as precipitant medium. In inert atmosphere, this process is normally carried out at comparatively very high temperatures, 70–90 °C [122]. The particles formed as a result of the process normally possess an arbitrary size and morphology. An additional constraint is connected to the accumulation trend in the coprecipitation agents. Particles of iron oxide can form large clusters owing to the anisotropic dipolar attraction, thereby displaying the particular properties connected to single-domain magnetic nanostructures [123].

Comparable studies are also found in other fields; for example, Roth et al. have investigated the impact of numerous experimental variables (e.g., reaction temperature, salt concentration, ratio of Fe^{3+}/Fe^{2+}, and ratio of hydroxide ions to iron ions). They focused largely on the influence of those variables on the size and the magnetization. In this respect, it was found that by adjusting the Fe^{2+}/Fe^{3+} ratio and raising the concentration of iron salts, the saturation magnetization can be improved. The concentration of iron salt and the ratio of hydroxide ions to iron ions affected the particle size [124].

Fang et al. estimated that by using the coprecipitation process, the MNP size was affected by the temperature and the base addition rate [125]. Quick mixing significantly affected the size of particles. It was also found that temperature further affected the size of particles. The influence of the variety of the base was observed by Mascolo et al. These writers tested three different types of base, $(C_2H_5)_4NOH$, NaOH, and KOH, carrying out coprecipitation at room temperature. They revealed a connection between the pH established in coprecipitation media and the tendency of magnetic nanoparticles to agglomerate. That pH is strongly influenced by the alkali nature [126].

The existence of additives, for instance surfactants, was an additional variable that has been widely studied. In this work, MNPs were manufactured by the process of coprecipitation and was improved using SDS in the postsynthesis step. Nanoparticles were consumed for the recovery and removal of nickel, zinc, and copper from industrial wastewater. This research showed that high adsorption capabilities might be obtained in less time thanks to the high surface area and also short diffusion route of SDS-coated Fe_3O_4 MNPs [127].

The current work was applied to perform a control of three significant properties of MNPs: surface change, shape, and size. The aim was to attain monodomain MNPs that were tunable by varying only the experimental conditions related to the methodology of preparation. Progress in nanotechnology is linked with nanoscale accuracy. MNPs are being used in an increasing number of commercial applications. The present work has the ability to control the crystallinity, shape, and size of MNPs and the development of new production methods [60, 128] by accurately adjusting the array magnitudes together with the crystallization of MNPs. The position and properties of MNPs on surfaces can be controlled using

biomineralization proteins. Naturally, complex synthetic functions are performed by proteins. Biomineralization proteins yield an inorganic mineral structure within biological organisms. Biomineralization proteins have been produced for millions of years to regulate the variety of ore below slightly aqueous states [7]. Numerous other biomineralizing biomolecules have been found or improved to prepare desirable materials in vitro and to shape the creation of abiotic materials (including silver, CoPt, and FePt [129–132].

Magnetotactic bacteria can develop extremely uniform MNPs constituted of magnetite, that is, magnetic iron oxide, Fe_3O_4, within the distinctive lipid organelles called magnetosomes. The crystallization of magnetite MNPs is controlled by the biomineralization proteins that remain inside the magnetosome membrane. Numerous proteins were discovered firmly bound to MNPs of the magnetite in the magnetotactic bacterium *Magnetospirillum magneticum* AMB-1 by Arakaki et al. [133]. One protein in particular, Mms6, comprises a hydrophobic N-terminal region for incorporation into the magnetosome membrane and an acidic C-terminal region that can powerfully fix iron ions; it is supposed to nucleate and regulate the development of magnetite in vivo [134]. It has also been revealed that refined Mms6 is able to regulate the development of MNPs of magnetite in vitro (Fig. 2.11) [135].

The method of synthesis of nanomaterials shows some very important measures that will regulate the particular size, size distribution, shape, the surface chemistry of particles, and, thus, their magnetic properties. The nanoparticles of iron oxide have been synthesized by a coprecipitation reaction between ferric and ferrous salts having inorganic bases, very strong bases, NaOH, and somewhat mild bases like NH_4OH. All these schemes indicate that magnetic behavior is similar to that of superparamagnetic materials. Using the aforementioned method, MNPs have been produced that are very small, 1–2 nm, and that have a precise uniform size; the standard deviation is less than 10%. A very uniform coating of silica (1 nm thin) is

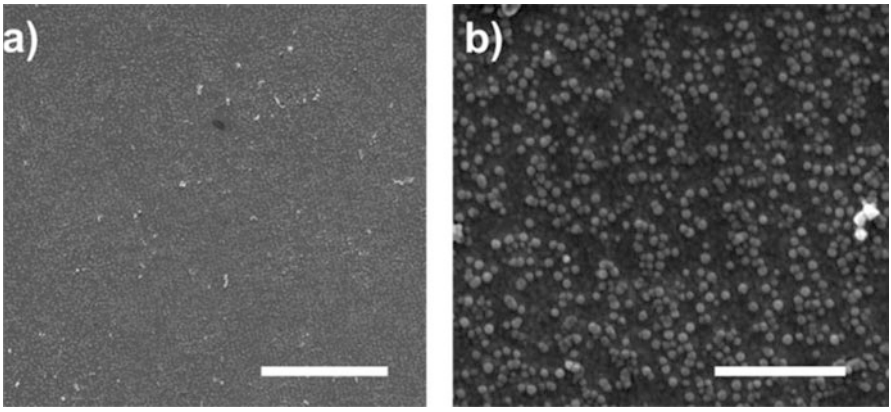

Fig. 2.11 SEM pictures of gold surfaces covered with whole layer of cysteine-tagged Mms6 protein patterned by interferometric lithography (IL) at a disclosure dose of 100 J cm^{-2}. Figure reprinted/adapted with permission from [136]

made using base-catalyzed hydrolysis and the reaction of polymerization of TEOS in microemulsion. It is very important to mention that the insignificant particle size of composites makes it a less acceptable candidate for in vivo applications [9].

2.5 Safety and Surface Stability of Magnetic Nanoparticles

The frequent use of nanomaterials in industrial and medical fields raises questions about their safe use and requires a comprehensive understanding of their life cycle in the body after exposure. Scientists claim that biodegradable nanoparticles are more suitable for biomedical applications because of their efficient metabolization. However, at the nanoscale, properties depend on the particles' size or shape (owing to a large surface-to-volume ratio) and as a result of physical and chemical transformations, the technologically relevant properties of nanoparticles can be changed drastically [137]. Therefore, it is important to provide an extensive understanding about the interactions of nanoparticles with biological environments. Additionally, the evaluation of degraded products is still very challenging owing to the complex phenomena in vivo [138]. For example, the dissolution of crystals can liberate toxic soluble ions, such as Fe^{2+} and Zn^{2+}. On the other hand, other factors, such as a coating polymer, can reduce crystal dissolution and increase the circulation time and persistence of nanoparticles. Recently various research groups have focused on these important issues to understand the life cycle of nanoparticles in vivo [139].

MNPs have less liberty for rotation and translation owing to dipole–dipole magnetic interactions at the cellular level. This reduces magnetic susceptibility and increases the blocking temperature. Consequently, the specific absorption rate of nanoparticles might fall after internalization if an AC magnetic field is applied. It is observed that degradation is a step-by-step dissolution process controlled by surface reaction processes. The physical transformations of nanoparticles indicate the loss of magnetic properties over time. Functionalization or coating of nanoparticles is one of the important factors used to control degradation mechanisms. Organic polymers or inorganic shells can be used as coating [140]. Organic polymers have been used to make nanoparticles biocompatible. This kind of polymer can also serve as a first barrier to control degradation. However, the nature and distribution of the polymer plays an important role in the dissolution of a crystal. An inorganic shell is also a potential candidate to control degradation mechanisms. For inorganic coatings, a complete shell is necessary to control the loss of the core part, in other words, a better cover rate of the core is an important factor. Additionally, an inorganic shell, for example gold, can lend its plasmon properties to nanoparticles. As a result, thermotherapy and plasmon therapy can be used simultaneously from a single nanoparticle. In conclusion, we need degradable nanoparticles, but the process of biodegradation should be delayed so that nanoparticles can be employed for the required application for a specified time [141].

2.6 Applications

2.6.1 Industrial Applications

Magnetic iron oxides (MIOs) are mostly used in porcelain, ceramics, and paints as synthetic pigments. They have attracted much attention in industry and other fields. These materials are attractive and useful in materials science and have vast applications in different fields [142, 143]. Both hematite and magnetite are used as catalysts for various reactions, for instance, in high-temperature water–gas shift reactions and in the preparation of ammonia. The synthesis of butadiene, the oxidation of alcohols, and Fishere–Tropsch synthesis for hydrocarbons are other reactions [144, 145].

2.6.2 Environmental Applications

For in situ applications, IONPs exhibit great flexibility. Supported and catalyzed NPs have been synthesized to increase their efficacy and speed of remediation [146]. Due to some unresolved ambiguities related to the use of IONPs, these substances are recognized as very useful tools in the rectification of various kinds of pollutants in air, soil, and water at both field and experimental levels [31]. Currently, various MNPs have been examined for the removal of both inorganic and organic contaminants.

2.6.3 Organic Pollutants

MNPs are used for the removal of excessive concentrations of organic mixtures [147, 148]. Dyes usually exist in wastewater flows in various branches of industry, for example, in the paint industry, tanneries, and textiles. Hence, MNPs could be suitable for the handling of textile waste.

2.6.4 Inorganic Pollutants

The main feature in metal toxin removal is the formation of functionalized sorbents for affinity or selective removal of harmful metal ions from complex matrices. For the removal of metal ions, MNPs are mostly used as sorbents. Because of the high surface area, MNPs exhibit high [149, 150] efficacy and ability in the removal of various metal ions. These results could be utilized to plan a suitable adsorption treatment for the recovery and removal of metal ions from wastewater.

2.6.5 Analytical Applications

1. *Fluorescence techniques*. Magnetic luminescent nanoparticles present a higher surface area-to-volume ratio owing to their small size than recently employed microbeads that result in faster reaction kinetics and an effective reaction homogeneity. Thus, the formation of magnetic fluorescent particles, such as silica nanoparticles embedded with quantum dots (QDs) and iron oxide, and Fe_2O_3 particles coated with dye-doped silica shells, shells of QDs or polystyrene magnetic beads with entrapped organic dyes or quantum dots [151], is quite simple. But, the application of MNPs is restricted generally to biological applications, for instance cellular imaging.
2. *Encapsulation of MNPs in polymeric matrixes*. The encapsulation of inorganic particles in organic polymers provides the particles with significant properties that bare, uncoated particles lack [152]. A polymer coating on these particles decreases their susceptibility to leaching, increases their compatibility with other organic constituents, and shields the surfaces of particles from oxidation.

   Encapsulation of MNPs in inorganic matrixes. Magnetic properties can be controlled by a simple heating method, and silica has been described to be an efficient approach to controlling magnetic properties [153]. A surface enriched in silica is indicative of surface silanol groups that can simply react with silane coupling agents and alcohols to produce dispersions [154].

2.6.6 Biomedical Applications

There are various biological and clinical applications of MNPs such as in vitro and in vivo applications. For in vivo applications, MNPs are used for diagnostic applications such as MRI as well as in therapies such as drug targeting and hyperthermia, while for in vitro applications, MNPs are mostly used in diagnostic selection, separation, and magnetorelaxometry [155, 156].

2.6.7 In Vivo Applications

For in vivo applications, two main factors, the surface and size functionality of MNPs, play a vital role. Even without affecting surface ligands, superparamagnetic iron oxide (SPIO) nanoparticle diameters greatly affect in vivo biodistribution. Ultrasmall SPIOs and particles with diameters 10–40 nm play a vital role for the prolonged circulation of blood [76].

1. *Therapeutic applications*. Hyperthermia: Employing SPIOs in varying-current magnetic fields arbitrarily reverses the direction of magnetization between both parallel and antiparallel directions. In the form of heat it allows for the transfer

of magnetic energy to particles. For in vivo applications, a property that can be used to enhance the temperature of malignant cells is known as hyperthermia. Cancerous cells are very responsive to an elevated temperature than healthy cells [157]. Also, the use of nanometer-sized magnetic particles is preferred instead of micron-sized magnetic particles because at reasonable AC magnetic fields, nanoparticles absorb much more power [158, 159], which is largely dependent on particle shape and size, and allows for the use of precise synthetic methods for fabricating uniform particles.

2. *Drug delivery*. For drug delivery, drug targeting is a very recent development. Over the last decade, the applications of IONPs in drug targeting have taken on great importance [160]. Magnetic NPs in combination with an external magnetic field allow for the delivery of particles to the required target locations, fix them at the local site while the medication is released, and act locally (magnetic drug targeting) [161]. The transport of drugs to a specific location can reduce side effects and diminish the required dose.

2.6.8 In Vitro Applications

1. *Diagnostic applications*

   a. *Separation and selection*. Currently solid-phase extraction has attracted a lot of attention. Solid phase extraction (SPE) is a technique to isolate and preconcentrate required constituents from a sample matrix. SPE is used for the determination of trace pollutants in ecological samples. Nowadays, nanoparticles have undergone significant advancements and have a considerable effect on sample extraction. This technique is considered the best substitute for the usual sample concentration processes [162–164].

   b. *Magnetorelaxometry*. Two relaxation procedures are Neel relaxation and Brownian relaxation. In Neel relaxation, the internal magnetization vector of the nanoparticles decreases in the direction of the axis inside the core [165]. In Brownian relaxation, particles achieve rotational diffusion in a carrier liquid. Brownian and Neel relaxation can be determined by their distinct relaxation times [166]. Moreover, Neel relaxation does not depend on the dispersal of nanoparticles, whereas Brownian relaxation occurs only in liquids, magnetorelaxometry is based on the hydrodynamic size and core size [167]. For magnetorelaxometry application, the advantage of decreasing the size of particles to the nanometer size is virtually identical to those explained for selection and separation applications.

   c. *MRI*. At the interface between medical diagnostics and nanomaterials, SPIO nanoparticles are treated as a group of new probes mostly suitable for both in vivo and in vitro molecular imaging as well as cellular imaging. In MRI, superparamagnetic contrast agents produce an increase in proton relaxation compared to paramagnetic contrast agents. Therefore, a smaller quantity of

SPIO agent is required to medicate the human body than a paramagnetic contrast agent. To relate the magnetic fluids to MRI contrast agents, the SPIO should be separated into biodegradable and biocompatible carriers.

d. *Bioseparation*. In biomedical research, for analysis it is required to separate the particular biological objects such as cells, DNAs, and proteins from their natural environment. In bioseparation applications, MNPs possess various excellent features owing to their high surface area and small size. In bioprocesses, SPIO nanoparticles have been mostly used for the purification and separation of biomolecules and cells [168–170].

2. *Catalysis applications*. Recently, catalysts supported by MNPs have been mostly used to compensate for the shortcomings of heterogeneous catalysis. Magnetic separation of catalysts in liquid-phase reactions is more reliable than centrifugation and cross-flow filtration, particularly when the catalysts are of submicrometer size. These small and magnetically divisible catalysts can combine high dispersal and reactivity with a simple separation process. The different kinds of transition metal–catalyzed reactions employing MNPs involve hydroformylation [171], carbon–carbon cross-coupling reactions, polymerization [172] reactions, and hydrogenation.

2.7 Future Prospects

Many reviews have been presented research related to the applications of SPIO nanoparticles as a contrast agent. MRI is not suitable for in situ monitoring. Thus, for in situ monitoring of nanoparticles in living cells a simple and precise approach is required. The use of nanometer-sized fluorescence probes is preferred over usual organic fluorescence probes in many application because they could produce good results by yielding strong fluorescence. The fluorescent signal can simply be affected by the background distortions produced by the matrix, and cells are the major issue in cell imaging employing fluorescent nanoprobes.

It is not easy to attain a high signal-to-noise ratio. Furthermore, it is still challenging to control the dynamics of MNPs and owing to these limitations precision is required. Specifically, it is important to have stepwise control over the synthesis process and understand the dynamics of MNPs and their behavior at each step.

The examples and techniques described in this section should be encouraging. In a pure way, various effective synthetic processes can be developed from these examples and techniques. These processes can be performed in a cost-effective way. The controlled synthesis of the nanostructure of nanomaterials can be attained using a simple method of perceiving theoretical principles and the molecular depiction of the retained systems. By easily varying the nature of the reacting species, the synthesis of MNPs by the various examples used in this section can be focused on the MNPs of all materials. Synthetic procedures have great potential in common applications.

In industry, more effort must be made to understand the structure of MNPs and to control the spatial distribution of nanomaterials. Further, novel and attractive nanomaterials could be synthesized by applying the latest microscopic techniques with new mixtures.

References

1. Grossman H, Myers W, Vreeland V, Bruehl R, Alper M, Bertozzi C, Clarke J (2004) Detection of bacteria in suspension by using a superconducting quantum interference device. Proc Natl Acad Sci 101:129–134
2. Chung S, Hoffmann A, Bader S, Liu C, Kay B, Makowski L, Chen L (2004) Biological sensors based on Brownian relaxation of magnetic nanoparticles. Appl Phys Lett 85:2971–2973
3. Duan F, Guojun J (2005) Introduction to condensed matter physics. World Scientific, Singapore
4. Ehrenreich H, Spaepen F (2001) Solid state physics. Academic Press
5. Néel L (1949) Effects of thermal fluctuations on the magnetization of small particles. CR Acad Sci Paris 228:1953
6. Néel L (1949) Theory of magnetic viscosity of fine grained ferromagnetics with application to baked clays. Ann Geophys 5:41
7. Leslie-Pelecky DL, Rieke RD (1996) Magnetic properties of nanostructured materials. Chem Mater 8:1770–1783
8. Morrish AH (2001) In: Morrish AH (ed) The physical principles of magnetism. Wiley-VCH, p 696. isbn:ISBN 0-7803-6029-X
9. Akbarzadeh A, Samiei M, Davaran S (2012) Magnetic nanoparticles: preparation, physical properties, and applications in biomedicine. Nanoscale Res Lett 7:1
10. Rümenapp C, Gleich B, Haase A (2012) Magnetic nanoparticles in magnetic resonance imaging and diagnostics. Pharm Res 29:1165–1179
11. Tang SC, Lo IM (2013) Magnetic nanoparticles: essential factors for sustainable environmental applications. Water Res 47:2613–2632
12. Colombo M, Carregal-Romero S, Casula MF, Gutierrez L, Morales MP, Boehm IB, Heverhagen JT, Prosperi D, Parak WJ (2012) Biological applications of magnetic nanoparticles. Chem Soc Rev 41:4306–4334
13. Sugimoto M (1999) The past, present, and future of ferrites. J Am Ceram Soc 82:269–280
14. Smit J, Wijn H (1954) Physical properties of ferrites. Adv Elect Electron Phys 6:69–136
15. Van Der Zaag P (1999) New views on the dissipation in soft magnetic ferrites. J Magn Magn Mater 196:315–319
16. Polking MJ, Alivisatos AP, Ramesh R (2015) Synthesis, physics, and applications of ferroelectric nanomaterials. MRS Commun 5:27–44
17. Hausner HH (2015) Modern materials: advances in development and applications. Elsevier, Amsterdam, Netherlands
18. Reddy DHK, Yun Y-S (2016) Spinel ferrite magnetic adsorbents: alternative future materials for water purification? Coord Chem Rev 315:90–111
19. Hill RJ, Craig JR, Gibbs G (1979) Systematics of the spinel structure type. Phys Chem Miner 4:317–339
20. Leem G, Sarangi S, Zhang S, Rusakova I, Brazdeikis A, Litvinov D, Lee TR (2009) Surfactant-controlled size and shape evolution of magnetic nanoparticles. Cryst Growth Des 9:32–34
21. Cornell RM, Schwertmann U (2003) The iron oxides: structure, properties, reactions, occurrences and uses. John Wiley & Sons, Hoboken, NJ

22. Gossuin Y, Gillis P, Hocq A, Vuong QL, Roch A (2009) Magnetic resonance relaxation properties of superparamagnetic particles. Wiley Interdiscip Rev Nanomed Nanobiotechnol 1:299–310
23. Rohrer GS (2001) Structure and bonding in crystalline materials. Cambridge University Press, Delhi
24. Stadelmann P (1987) EMS-a software package for electron diffraction analysis and HREM image simulation in materials science. Ultramicroscopy 21:131–145
25. Jang JT, Nah H, Lee JH, Moon SH, Kim MG, Cheon J (2009) Critical enhancements of MRI contrast and hyperthermic effects by dopant-controlled magnetic nanoparticles. Angew Chem 121:1260–1264
26. Kang E, Park J, Hwang Y, Kang M, Park J-G, Hyeon T (2004) Direct synthesis of highly crystalline and monodisperse manganese ferrite nanocrystals. J Phys Chem B 108:13932–13935
27. Song Q, Zhang ZJ (2004) Shape control and associated magnetic properties of spinel cobalt ferrite nanocrystals. J Am Chem Soc 126:6164–6168
28. Tromsdorf UI, Bigall NC, Kaul MG, Bruns OT, Nikolic MS, Mollwitz B, Sperling RA, Reimer R, Hohenberg H, Parak WJ (2007) Size and surface effects on the MRI relaxivity of manganese ferrite nanoparticle contrast agents. Nano Lett 7:2422–2427
29. Dronskowski R (2001) The little maghemite story: a classic functional material. Adv Funct Mater 11:27–29
30. Lévy M, Wilhelm C, Siaugue J-M, Horner O, Bacri J-C, Gazeau F (2008) Magnetically induced hyperthermia: size-dependent heating power of γ-Fe_2O_3 nanoparticles. J Phys Condens Matter 20:204133
31. Waychunas GA (1991) Crystal chemistry of oxides and oxyhydroxides. Rev Mineral Geochem 25:11–68
32. Chen T, Xu H, Ji J, Chen J, Chen Y (2003) Formation mechanism of ferromagnetic minerals in loess of China: TEM investigation. Chin Sci Bull 48:2260–2267
33. Matijevic E, Good RJ (2012) Surface and colloid science. Springer, Berlin
34. Klahr BM, Martinson AB, Hamann TW (2010) Photoelectrochemical investigation of ultrathin film iron oxide solar cells prepared by atomic layer deposition. Langmuir 27:461–468
35. Saremi-Yarahmadi S, Wijayantha KGU, Tahir AA, Vaidhyanathan B (2009) Nanostructured α-Fe2O3 electrodes for solar driven water splitting: effect of doping agents on preparation and performance. J Phys Chem C 113:4768–4778
36. Wu C, Yin P, Zhu X, Ouyang C, Xie Y (2006) Synthesis of hematite (α-Fe2O3) nanorods: diameter-size and shape effects on their applications in magnetism, lithium ion battery, and gas sensors. J Phys Chem B 110:17806–17812
37. Zeng S, Tang K, Li T, Liang Z, Wang D, Wang Y, Zhou W (2007) Hematite hollow spindles and microspheres: selective synthesis, growth mechanisms, and application in lithium ion battery and water treatment. J Phys Chem C 111:10217–10225
38. Zhang G, Gao Y, Zhang Y, Guo Y (2010) Fe_2O_3-pillared rectorite as an efficient and stable Fenton-like heterogeneous catalyst for photodegradation of organic contaminants. Environ Sci Technol 44:6384–6389
39. Cheng C-J, Lin C-C, Chiang R-K, Lin C-R, Lyubutin IS, Alkaev EA, Lai H-Y (2008) Synthesis of monodisperse magnetic iron oxide nanoparticles from submicrometer hematite powders. Crystal Growth Design 8:877–883
40. Morrish AH (1994) Canted antiferromagnetism: hematite. World Scientific, Singapore
41. Cameron AG (1973) Abundances of the elements in the solar system. Space Sci Rev 15:121–146
42. Suess HE, Urey HC (1956) Abundances of the elements. Rev Mod Phys 28:53
43. Fleischer RL, Price PB, Walker RM (1975) Nuclear tracks in solids: principles and applications. University of California Press, Berkeley, CA
44. Ngo A, Pileni M (2001) Assemblies of ferrite nanocrystals: partial orientation of the easy magnetic axes. J Phys Chem B 105:53–58

45. Raj K, Moskowitz B, Casciari R (1995) Advances in ferrofluid technology. J Magn Magn Mater 149:174–180
46. Singhal S, Singh J, Barthwal S, Chandra K (2005) Preparation and characterization of nanosize nickel-substituted cobalt ferrites (Co 1− xNixFe$_2$O$_4$). J Solid State Chem 178:3183–3189
47. Sousa MH, Tourinho FA, Depeyrot J, Da Silva GJ, Lara MCF (2001) New electric double-layered magnetic fluids based on copper, nickel, and zinc ferrite nanostructures. J Phys Chem B 105:1168–1175
48. Rooksby H, Willis B (1953) Crystal structure and magnetic properties of cobalt ferrite at low temperatures.
49. Thanh NT, Maclean N, Mahiddine S (2014) Mechanisms of nucleation and growth of nanoparticles in solution. Chem Rev 114:7610–7630
50. Fanun M (2016) Colloids in drug delivery. CRC Press, Boca Raton, FL
51. Liveri VT (2006) Nucleation, growth, and arrested growth in confined space. In: Controlled synthesis of nanoparticles in microheterogeneous systems. Springer, New York, pp 75–90
52. Marchal P, David R, Klein J, Villermaux J (1988) Crystallization and precipitation engineering—I. An efficient method for solving population balance in crystallization with agglomeration. Chem Eng Sci 43:59–67
53. Mersmann A (1999) Crystallization and precipitation. Chem Eng Process Process Intensif 38:345–353
54. Dirksen J, Ring T (1991) Fundamentals of crystallization: kinetic effects on particle size distributions and morphology. Chem Eng Sci 46:2389–2427
55. Franke J, Mersmann A (1995) The influence of the operational conditions on the precipitation process. Chem Eng Sci 50:1737–1753
56. Costa CBB, Maciel MRW, Maciel Filho R (2007) Considerations on the crystallization modeling: population balance solution. Comput Chem Eng 31:206–218
57. Banfield JF, Zhang H (2001) Nanoparticles in the environment. Rev Mineral Geochem 44:1–58
58. Pascal C, Pascal J, Favier F, Elidrissi Moubtassim M, Payen C (1999) Electrochemical synthesis for the control of γ-Fe2O3 nanoparticle size. Morphology, microstructure, and magnetic behavior. Chem Mater 11:141–147
59. Cote LJ, Teja AS, Wilkinson AP, Zhang ZJ (2002) Continuous hydrothermal synthesis and crystallization of magnetic oxide nanoparticles. J Mater Res 17:2410–2416
60. Laurent S, Forge D, Port M, Roch A, Robic C, Vander Elst L, Muller RN (2008) Magnetic iron oxide nanoparticles: synthesis, stabilization, vectorization, physicochemical characterizations, and biological applications. Chem Rev 108:2064–2110
61. Hua CC, Zakaria S, Farahiyan R, Khong LT (2008) Size-controlled synthesis and characterization of Fe. Sains Malaysiana 37:389–394
62. Mehnert W, Mäder K (2001) Solid lipid nanoparticles: production, characterization and applications. Adv Drug Deliv Rev 47:165–196
63. Sun L, Huang C, Gong T, Zhou S (2010) A biocompatible approach to surface modification: biodegradable polymer functionalized super-paramagnetic iron oxide nanoparticles. Mater Sci Eng C 30:583–589
64. Marciano V, Minore A, Liveri VT (2000) A simple method to prepare solid nanoparticles of water-soluble salts using water-in-oil microemulsions. Colloid Polym Sci 278:250–252
65. Chen D, Tang X, Wu J, Zhang W, Liu Q, Jiang Y (2011) Effect of grain size on the magnetic properties of superparamagnetic Ni 0.5 Zn 0.5 Fe$_2$O$_4$ nanoparticles by co-precipitation process. J Magn Magn Mater 323:1717–1721
66. Wilson K, Harris L, Goff J, Riffle J, Dailey J (2002) A generalized method for magnetite nanoparticle steric stabilization utilizing block copolymers containing carboxylic acids. Eur Cell Mater 3:206–209
67. Levy L, Hochepied J, Pileni M (1996) Control of the size and composition of three dimensionally diluted magnetic semiconductor clusters. J Phys Chem 100:18322–18326

68. Wang W, Efrima S, Regev O (1999) Directing silver nanoparticles into colloid-surfactant lyotropic lamellar systems. J Phys Chem B 103:5613–5621
69. Qi L, Gao Y, Ma J (1999) Synthesis of ribbons of silver nanoparticles in lamellar liquid crystals. Colloids Surf A Physicochem Eng Asp 157:285–294
70. Andersson M, Alfredsson V, Kjellin P, Palmqvist AE (2002) Macroscopic alignment of silver nanoparticles in reverse hexagonal liquid crystalline templates. Nano Lett 2:1403–1407
71. Liveri VT (2006) Controlled synthesis of nanoparticles in microheterogeneous systems. Springer, Berlin
72. Wu S-H, Chen D-H (2004) Synthesis of high-concentration Cu nanoparticles in aqueous CTAB solutions. J Colloid Interface Sci 273:165–169
73. Rabatic BM, Pralle MU, Tew GN, Stupp SI (2003) Nanostructured semiconductors templated by cholesteryl-oligo (ethylene oxide) amphiphiles. Chem Mater 15:1249–1255
74. Yang H, Guo R, Wang H (2001) Lubrication of the mixed system of Triton X-100/n-C 10 H 21 OH/H_2O lamellar liquid crystal and ZnS nanoparticles. Colloids Surf A Physicochem Eng Asp 180:243–251
75. Padhi A, Nanjundaswamy K, Masquelier C, Okada S, Goodenough J (1997) Effect of structure on the Fe^{3+}/Fe^{2+} redox couple in iron phosphates. J Electrochem Soc 144:1609–1613
76. Lu AH, Salabas EEL, Schüth F (2007) Magnetic nanoparticles: synthesis, protection, functionalization, and application. Angew Chem Int Ed 46:1222–1244
77. Park BK, Jeong S, Kim D, Moon J, Lim S, Kim JS (2007) Synthesis and size control of monodisperse copper nanoparticles by polyol method. J Colloid Interface Sci 311:417–424
78. Faraji M, Yamini Y, Saleh A, Rezaee M, Ghambarian M, Hassani R (2010) A nanoparticle-based solid-phase extraction procedure followed by flow injection inductively coupled plasma-optical emission spectrometry to determine some heavy metal ions in water samples. Anal Chim Acta 659:172–177
79. Ramimoghadam D, Bagheri S, Hamid SBA (2014) Progress in electrochemical synthesis of magnetic iron oxide nanoparticles. J Magn Magn Mater 368:207–229
80. Cabrera L, Gutierrez S, Menendez N, Morales M, Herrasti P (2008) Magnetite nanoparticles: electrochemical synthesis and characterization. Electrochim Acta 53:3436–3441
81. Teja AS, Koh P-Y (2009) Synthesis, properties, and applications of magnetic iron oxide nanoparticles. Prog Cryst Growth Charact Mater 55:22–45
82. Suwalka O, Sharma RK, Sebastian V, Lakshmi N, Venugopalan K (2007) A study of nanosized Ni substituted Co–Zn ferrite prepared by coprecipitation. J Magn Magn Mater 313:198–203
83. Wu W, Wu Z, Yu T, Jiang C, Kim W-S (2016) Recent progress on magnetic iron oxide nanoparticles: synthesis, surface functional strategies and biomedical applications. Sci Technol Adv Mater 16(2):023501
84. Massart R (1981) Preparation of aqueous magnetic liquids in alkaline and acidic media. IEEE Trans Magn 17:1247–1248
85. Wei W, Quanguo H, Rong H, Jingke H, Hong C (2007) Preparation and characterization of magnetite Fe3O4 nanopowders. Rare Metal Mater Eng 36:238–243
86. Azcona P, Zysler R, Lassalle V (2016) Simple and novel strategies to achieve shape and size control of magnetite nanoparticles intended for biomedical applications. Colloids Surf A Physicochem Eng Asp 504:320–330
87. Morales MDP, Veintemillas-Verdaguer S, Montero M, Serna C, Roig A, Casas L, Martinez B, Sandiumenge F (1999) Surface and internal spin canting in γ-Fe_2O_3 nanoparticles. Chem Mater 11:3058–3064
88. Sugimoto T (1987) Preparation of monodispersed colloidal particles. Adv Colloid Interf Sci 28:65–108
89. Boistelle R, Astier J (1988) Crystallization mechanisms in solution. J Cryst Growth 90:14–30
90. Jolivet J, Henry M, Livage J (2000) Metal oxide chemistry and synthesis: from solution to oxide. Wiley, New York

91. Babes L, Denizot BT, Tanguy G, Le Jeune JJ, Jallet P (1999) Synthesis of iron oxide nanoparticles used as MRI contrast agents: a parametric study. J Colloid Interface Sci 212:474–482
92. Jiang W, Yang H-C, Yang S-Y, Horng H-E, Hung J, Chen Y, Hong C-Y (2004) Preparation and properties of superparamagnetic nanoparticles with narrow size distribution and biocompatible. J Magn Magn Mater 283:210–214
93. Tartaj P, González-Carreño T, Serna CJ (2004) From hollow to dense spheres: control of dipolar interactions by tailoring the architecture in colloidal aggregates of superparamagnetic iron oxide nanocrystals. Adv Mater 16:529–533
94. Wang X, Zhuang J, Peng Q, Li Y (2005) A general strategy for nanocrystal synthesis. Nature 437:121–124
95. Anderson SA, Rader RK, Westlin WF, Null C, Jackson D, Lanza GM, Wickline SA, Kotyk JJ (2000) Magnetic resonance contrast enhancement of neovasculature with αvβ3-targeted nanoparticles. Magn Reson Med 44:433–439
96. Khollam Y, Dhage S, Potdar H, Deshpande S, Bakare P, Kulkarni S, Date S (2002) Microwave hydrothermal preparation of submicron-sized spherical magnetite (Fe_3O_4) powders. Mater Lett 56:571–577
97. Kasapoğlu N, Baykal A, Toprak MS, Köseoğlu Y, Bayrakdar H (2007) Synthesis and characterization of $NiFe_2O_4$ nano-octahedrons by EDTA-assisted hydrothermal method. Turk J Chem 31:659–666
98. Wang G, Shen X, Horvat J, Wang B, Liu H, Wexler D, Yao J (2009) Hydrothermal synthesis and optical, magnetic, and supercapacitance properties of nanoporous cobalt oxide nanorods. J Phys Chem C 113:4357–4361
99. Kadier W, Sadeh B, Duamet B, Aman M (2014) Hydrothermal synthesis and properties of CoFe2O4 magnetic nanoparticles 31.
100. Haw CY, Mohamed F, Chia CH, Radiman S, Zakaria S, Huang NM, Lim HN (2010) Hydrothermal synthesis of magnetite nanoparticles as MRI contrast agents. Ceram Int 36:1417–1422
101. Nejati K, Zabihi R (2012) Preparation and magnetic properties of nano size nickel ferrite particles using hydrothermal method. Chem Cent J 6:1
102. Tartaj P, Del Puerto MM, Veintemillas-Verdaguer S, González-Carreño T, Serna CJ (2003) The preparation of magnetic nanoparticles for applications in biomedicine. J Phys D Appl Phys 36:R182
103. Sugimoto T (2000) Fine particles: synthesis, characterization, and mechanisms of growth. CRC Press, Boca Raton, FL
104. Cai W, Wan J (2007) Facile synthesis of superparamagnetic magnetite nanoparticles in liquid polyols. J Colloid Interface Sci 305:366–370
105. Viau G, Ravel F, Acher O, Fiévet-Vincent F, Fiévet F (1994) Preparation and microwave characterization of spherical and monodisperse Co20Ni80 particles. J Appl Phys 76:6570–6572
106. Majidi S, Zeinali Sehrig F, Farkhani SM, Soleymani Goloujeh M, Akbarzadeh A (2016) Current methods for synthesis of magnetic nanoparticles. Artificial Cells Nanomed Biotechnol 44:722–734
107. Viau G, Fievet-Vincent F, Fievet F (1996) Monodisperse iron-based particles: precipitation in liquid polyols. J Mater Chem 6:1047–1053
108. Fievet F, Lagier J, Blin B, Beaudoin B, Figlarz M (1989) Homogeneous and heterogeneous nucleations in the polyol process for the preparation of micron and submicron size metal particles. Solid State Ionics 32:198–205
109. Tzitzios V, Petridis D, Zafiropoulou I, Hadjipanayis G, Niarchos D (2005) Synthesis and characterization of L1 0 FePt nanoparticles from Pt–Fe_3O_4 core-shell nanoparticles. J Magn Magn Mater 294:e95–e98
110. Jezequel D, Guenot J, Jouini N, Fievet F (1995) Submicrometer zinc oxide particles: elaboration in polyol medium and morphological characteristics. J Mater Res 10:77–83

111. Liu J, Qiao SZ, Hu QH (2011) Magnetic nanocomposites with mesoporous structures: synthesis and applications. Small 7:425–443
112. Reetz MT, Helbig W, Quaiser SA (1996) Electrochemical methods in the synthesis of nanostructured transition metal clusters. Active Metals Prep Charact Appl:279–297
113. Khan H, Petrikowski K (2000) Anisotropic structural and magnetic properties of arrays of Fe 26 Ni 74 nanowires electrodeposited in the pores of anodic alumina. J Magn Magn Mater 215:526–528
114. Pankhurst Q, Thanh N, Jones S, Dobson J (2009) Progress in applications of magnetic nanoparticles in biomedicine. J Phys D Appl Phys 42:224001
115. Salazar-Alvarez G, Muhammed M, Zagorodni AA (2006) Novel flow injection synthesis of iron oxide nanoparticles with narrow size distribution. Chem Eng Sci 61:4625–4633
116. Pankhurst QA, Connolly J, Jones SK, Dobson J (2003) Applications of magnetic nanoparticles in biomedicine. J Phys D Appl Phys 36:R167
117. Rodríguez-López A, Cruz-Rivera J, Elías-Alfaro C, Betancourt I, Ruiz-Silva H, Antaño-López R (2015) Fine tuning of magnetite nanoparticle size distribution using dissymmetric potential pulses in the presence of biocompatible surfactants and the electrochemical characterization of the nanoparticles. Mater Sci Eng C 46:538–547
118. Chatterjee K, Sarkar S, Rao KJ, Paria S (2014) Core/shell nanoparticles in biomedical applications. Adv Colloid Interf Sci 209:8–39
119. Herea D, Chiriac H, Lupu N, Grigoras M, Stoian G, Stoica B, Petreus T (2015) Study on iron oxide nanoparticles coated with glucose-derived polymers for biomedical applications. Appl Surf Sci 352:117–125
120. Khoee S, Shagholani H, Abedini N (2015) Synthesis of quasi-spherical and square shaped oligoamino-ester graft-from magnetite nanoparticles: effect of morphology and chemical structure on protein interactions. Polymer 56:207–217
121. Calatayud MP, Sanz B, Raffa V, Riggio C, Ibarra MR, Goya GF (2014) The effect of surface charge of functionalized Fe 3 O 4 nanoparticles on protein adsorption and cell uptake. Biomaterials 35:6389–6399
122. Šutka A, Lagzdina S, Käämbre T, Pärna R, Kisand V, Kleperis J, Maiorov M, Kikas A, Kuusik I, Jakovlevs D (2015) Study of the structural phase transformation of iron oxide nanoparticles from an Fe2+ ion source by precipitation under various synthesis parameters and temperatures. Mater Chem Phys 149–150:473–479
123. Lassalle V, Avena M, Ferreira M (2009) A review of the methods of magnetic nanocomposites synthesis and their applications as drug delivery systems and immobilization supports for lipases. Current Trends Polymer Sci 13:37–67
124. Roth H-C, Schwaminger SP, Schindler M, Wagner FE, Berensmeier S (2015) Influencing factors in the c-precipitation process of superparamagnetic iron oxide nano particles: a model based study. J Magn Magn Mater 377:81–89
125. Fang M, Ström V, Olsson RT, Belova L, Rao KV (2012) Particle size and magnetic properties dependence on growth temperature for rapid mixed co-precipitated magnetite nanoparticles. Nanotechnology 23:145601
126. Mascolo MC, Pei Y, Ring TA (2013) Room temperature co-precipitation synthesis of magnetite nanoparticles in a large pH window with different bases. Materials 6:5549–5567
127. Adeli M, Yamini Y, Faraji M (2012) Removal of copper, nickel and zinc by sodium dodecyl sulphate coated magnetite nanoparticles from water and wastewater samples. Arab J Chem. doi:10.1016/j.arabjc.2012.10.012
128. Reddy LH, Arias JL, Nicolas J, Couvreur P (2012) Magnetic nanoparticles: design and characterization, toxicity and biocompatibility, pharmaceutical and biomedical applications. Chem Rev 112:5818–5878
129. Wang B, Chen K, Jiang S, Reincke F, Tong W, Wang D, Gao C (2006) Chitosan-mediated synthesis of gold nanoparticles on patterned poly (dimethylsiloxane) surfaces. Biomacromolecules 7:1203–1209
130. Naik RR, Stringer SJ, Agarwal G, Jones SE, Stone MO (2002) Biomimetic synthesis and patterning of silver nanoparticles. Nat Mater 1:169–172

131. Reiss BD, Mao C, Solis DJ, Ryan KS, Thomson T, Belcher AM (2004) Biological routes to metal alloy ferromagnetic nanostructures. Nano Lett 4:1127–1132
132. Galloway JM, Bird SM, Bramble JP, Critchley K, Staniland SS (2013) Biotemplating magnetic nanoparticles on patterned surfaces for potential use in data storage. In: MRS Proceedings. Cambridge University Press, Delhi, pp 231–237
133. Arakaki A, Webb J, Matsunaga T (2003) A novel protein tightly bound to bacterial magnetic particles in Magnetospirillum magneticum strain AMB-1. J Biol Chem 278:8745–8750
134. Galloway JM, Arakaki A, Masuda F, Tanaka T, Matsunaga T, Staniland SS (2011) Magnetic bacterial protein Mms6 controls morphology, crystallinity and magnetism of cobalt-doped magnetite nanoparticles in vitro. J Mater Chem 21:15244–15254
135. Wang L, Prozorov T, Palo PE, Liu X, Vaknin D, Prozorov R, Mallapragada S, Nilsen-Hamilton M (2011) Self-assembly and biphasic iron-binding characteristics of Mms6, a bacterial protein that promotes the formation of superparamagnetic magnetite nanoparticles of uniform size and shape. Biomacromolecules 13:98–105
136. Bird SM, El-Zubir O, Rawlings AE, Leggett GJ, Staniland SS (2016) A novel design strategy for nanoparticles on nanopatterns: interferometric lithographic patterning of Mms6 biotemplated magnetic nanoparticles. J Mater Chem C 4:3948–3955
137. Kolosnjaj-Tabi J, Lartigue L, Javed Y, Luciani N, Pellegrino T, Wilhelm C, Alloyeau D, Gazeau F (2016) Biotransformations of magnetic nanoparticles in the body. Nano Today 11(3):280–284
138. Lartigue L, Alloyeau D, Kolosnjaj-Tabi J, Javed Y, Guardia P, Riedinger A, Péchoux C, Pellegrino T, Wilhelm C, Gazeau F (2013) Biodegradation of iron oxide nanocubes: high-resolution in situ monitoring. ACS Nano 7:3939–3952
139. Javed Y, Lartigue L, Hugounenq P, Vuong QL, Gossuin Y, Bazzi R, Wilhelm C, Ricolleau C, Gazeau F, Alloyeau D (2014) Biodegradation mechanisms of iron oxide monocrystalline nanoflowers and tunable shield effect of gold coating. Small 10:3325–3337
140. Mazuel F, Espinosa A, Luciani N, Reffay M, Le Borgne R, Motte L, Desboeufs K, Michel A, Pellegrino T, Lalatonne Y (2016) Massive intracellular biodegradation of iron oxide nanoparticles evidenced magnetically at single endosome and tissue levels. ACS Nano 10(8):7627–7638
141. Kolosnjaj-Tabi J, Javed Y, Lartigue L, Volatron J, Elgrabli D, Marangon I, Pugliese G, Caron B, Figuerola A, Luciani N (2015) The one year fate of iron oxide coated gold nanoparticles in mice. ACS Nano 9:7925–7939
142. Jun YW, Choi JS, Cheon J (2006) Shape control of semiconductor and metal oxide nanocrystals through nonhydrolytic colloidal routes. Angew Chem Int Ed 45:3414–3439
143. Nunez NO, Tartaj P, Morales MP, Pozas R, Ocana M, Serna CJ (2003) Preparation, characterization, and magnetic properties of Fe-based alloy particles with elongated morphology. Chem Mater 15:3558–3563
144. Park S-J, Kim S, Lee S, Khim ZG, Char K, Hyeon T (2000) Synthesis and magnetic studies of uniform iron nanorods and nanospheres. J Am Chem Soc 122:8581–8582
145. Dumestre F, Chaudret B, Amiens C, Renaud P, Fejes P (2004) Superlattices of iron nanocubes synthesized from Fe [N (SiMe3) 2] 2. Science 303:821–823
146. Wang L, Luo J, Fan Q, Suzuki M, Suzuki IS, Engelhard MH, Lin Y, Kim N, Wang JQ (2005) Monodispersed core-shell Fe3O4@ Au nanoparticles. J Phys Chem B 109:21593–21601
147. Caruntu D, Cushing BL, Caruntu G, O'connor CJ (2005) Attachment of gold nanograins onto colloidal magnetite nanocrystals. Chem Mater 17:3398–3402
148. Lyon JL, Fleming DA, Stone MB, Schiffer P, Williams ME (2004) Synthesis of Fe oxide core/Au shell nanoparticles by iterative hydroxylamine seeding. Nano Lett 4:719–723
149. Zambaux M, Bonneaux F, Gref R, Dellacherie E, Vigneron C (1999) Preparation and characterization of protein C-loaded PLA nanoparticles. J Control Release 60:179–188
150. Stolnik S, Illum L, Davis S (1995) Long circulating microparticulate drug carriers. Adv Drug Deliv Rev 16:195–214

151. Savva M, Duda E, Huang L (1999) A genetically modified recombinant tumor necrosis factor-α conjugated to the distal terminals of liposomal surface grafted polyethyleneglycol chains. Int J Pharm 184:45–51
152. Peracchia MT, Vauthier C, Passirani C, Couvreur P, Labarre D (1997) Complement consumption by poly (ethylene glycol) in different conformations chemically coupled to poly (isobutyl 2-cyanoacrylate) nanoparticles. Life Sci 61:749–761
153. Sah H (1999) Stabilization of proteins against methylene chloride/water interface-induced denaturation and aggregation. J Control Release 58:143–151
154. Velge-Roussel F, Breton P, Guillon X, Lescure F, Bru N, Bout D, Hoebeke J (1996) Immunochemical characterization of antibody-coated nanoparticles. Experientia 52:803–806
155. Piao Y, Kim J, Na HB, Kim D, Baek JS, Ko MK, Lee JH, Shokouhimehr M, Hyeon T (2008) Wrap–bake–peel process for nanostructural transformation from β-FeOOH nanorods to biocompatible iron oxide nanocapsules. Nat Mater 7:242–247
156. Liu C, Wu X, Klemmer T, Shukla N, Weller D, Roy AG, Tanase M, Laughlin D (2005) Reduction of sintering during annealing of FePt nanoparticles coated with iron oxide. Chem Mater 17:620–625
157. Mikhaylova M, Kim DK, Bobrysheva N, Osmolowsky M, Semenov V, Tsakalakos T, Muhammed M (2004) Superparamagnetism of magnetite nanoparticles: dependence on surface modification. Langmuir 20:2472–2477
158. Jeong U, Teng X, Wang Y, Yang H, Xia Y (2007) Superparamagnetic colloids: controlled synthesis and niche applications. Adv Mater 19:33–60
159. Hyeon T (2003) Chemical synthesis of magnetic nanoparticles. Chem Commun:927–934
160. Casula MF, Jun Y-W, Zaziski DJ, Chan EM, Corrias A, Alivisatos AP (2006) The concept of delayed nucleation in nanocrystal growth demonstrated for the case of iron oxide nanodisks. J Am Chem Soc 128:1675–1682
161. Kwon SG, Piao Y, Park J, Angappane S, Jo Y, Hwang N-M, Park J-G, Hyeon T (2007) Kinetics of monodisperse iron oxide nanocrystal formation by "heating-up" process. J Am Chem Soc 129:12571–12584
162. Dubertret B, Skourides P, Norris DJ, Noireaux V, Brivanlou AH, Libchaber A (2002) In vivo imaging of quantum dots encapsulated in phospholipid micelles. Science 298:1759–1762
163. Gao X, Cui Y, Levenson RM, Chung LW, Nie S (2004) In vivo cancer targeting and imaging with semiconductor quantum dots. Nat Biotechnol 22:969–976
164. Pellegrino T, Manna L, Kudera S, Liedl T, Koktysh D, Rogach AL, Keller S, Rädler J, Natile G, Parak WJ (2004) Hydrophobic nanocrystals coated with an amphiphilic polymer shell: a general route to water soluble nanocrystals. Nano Lett 4:703–707
165. White MA, Johnson JA, Koberstein JT, Turro NJ (2006) Toward the syntheses of universal ligands for metal oxide surfaces: controlling surface functionality through click chemistry. J Am Chem Soc 128:11356–11357
166. Caruso F (2001) Nanoengineering of particle surfaces. Adv Mater 13:11–22
167. Stöber W, Fink A, Bohn E (1968) Controlled growth of monodisperse silica spheres in the micron size range. J Colloid Interface Sci 26:62–69
168. Yi DK, Selvan ST, Lee SS, Papaefthymiou GC, Kundaliya D, Ying JY (2005) Silica-coated nanocomposites of magnetic nanoparticles and quantum dots. J Am Chem Soc 127:4990–4991
169. Yi DK, Lee SS, Papaefthymiou GC, Ying JY (2006) Nanoparticle architectures templated by SiO2/Fe2O3 nanocomposites. Chem Mater 18:614–619
170. Kim J, Lee JE, Lee J, Yu JH, Kim BC, An K, Hwang Y, Shin C-H, Park J-G, Kim J (2006) Magnetic fluorescent delivery vehicle using uniform mesoporous silica spheres embedded with monodisperse magnetic and semiconductor nanocrystals. J Am Chem Soc 128:688–689
171. Yoon TJ, Yu KN, Kim E, Kim JS, Kim BG, Yun SH, Sohn BH, Cho MH, Lee JK, Park SB (2006) Specific targeting, cell sorting, and bioimaging with smart magnetic silica core–shell nanomaterials. Small 2:209–215
172. Yoon T-J, Kim JS, Kim BG, Yu KN, Cho M-H, Lee J-K (2005) Multifunctional nanoparticles possessing a "magnetic motor effect" for drug or gene delivery. Angew Chem Int Ed 44:1068–1071